

Simulation of Models and Algorithms for Wireless Communication Systems

by

Imad W. Jabbour

B.E., Computer and Communications Engineering
American University of Beirut (2005)

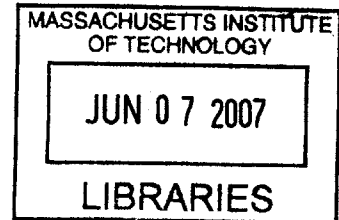
Submitted to the Department of Civil and Environmental Engineering
in partial fulfillment of the requirements for the degree of

Master of Science

at the

MASSACHUSETTS INSTITUTE OF TECHNOLOGY

June 2007



© Massachusetts Institute of Technology 2007. All rights reserved.

A handwritten signature in black ink, appearing to be "Imad W. Jabbour".

Author
Department of Civil and Environmental Engineering
April 19, 2007

Certified by
Lizhong Zheng
Associate Professor, Electrical Engineering and Computer Science
Thesis Supervisor

Read by
Steven R. Lerman
Professor, Civil and Environmental Engineering
Thesis Reader

A small handwritten mark, possibly a checkmark or the number "11".

Accepted by
Daniele Veneziano
Chairman, Departmental Committee for Graduate Students

BARKER

Simulation of Models and Algorithms for Wireless Communication Systems

by

Imad W. Jabbour

Submitted to the Department of Civil and Environmental Engineering
on April 19, 2007, in partial fulfillment of the
requirements for the degree of
Master of Science

Abstract

The thesis presents a set of simulations of models and algorithms for wireless communication systems. The simulations are developed using graphical MATLAB interfaces, and cover the fundamentals of wireless channel modeling, the advantages and limitations of antenna beamforming in multiuser systems, and the underlying principles of OFDM. The thesis targets two types of audiences in particular: students and wireless industry professionals. For the former, it constitutes an excellent complement to lecture notes, and for the latter, it is an efficient way to review the key principles and technologies. In either case, the simulations provide an intuitive view of the addressed topics, thus allowing users to comprehend the basics of wireless channels and phenomena without delving into mathematical complexities.

Thesis Supervisor: Lizhong Zheng

Title: Associate Professor, Electrical Engineering and Computer Science

Thesis Reader: Steven R. Lerman

Title: Professor, Civil and Environmental Engineering

Acknowledgments

First and foremost, I would like to thank my parents for their love and sacrifice. I wouldn't have overcome the difficulties I faced while at MIT, without their continuous support. They are my true blessing.

I am grateful to my thesis supervisor, Prof. Lizhong Zheng for introducing me to LIDS and for proposing this problem and guiding me through it. His comments were always insightful and he helped me channel my efforts in the correct direction.

I am thankful to Prof. Steven Lerman for reading this thesis. Steve was an invaluable academic advisor and his discerning remarks and guidance made my academic journey much simpler and more effective.

Before joining LIDS, I worked for almost two years at CECI. I would like to thank the iLabs team at CECI: Jud Harward, Phil Bailey, Kirky DeLong and Tingting Mao. I am particularly grateful to Jud, whom I had the pleasure of interacting with as an intern, research assistant, and most of all as a friend. The rest of the folks at CECI were fantastic: Mike Danziger, Mark Bessette, Maria Karatzas, Andrew McKinney and of course, Meg Westlund. They all made my stay at CECI extremely pleasant.

More personally, I am grateful to Mesrob Ohannessian, Rabih Zbib, Loai Naamani and Deena Sharuk, for their friendship and their advice in countless situations.

Contents

| | | |
|----------|---|-----------|
| 1 | Introduction | 11 |
| 1.1 | Overview and Motivation | 11 |
| 1.2 | Thesis Organization | 12 |
| 2 | The Wireless Channel | 13 |
| 2.1 | Modeling of Wireless Channels | 13 |
| 2.1.1 | Transmit-Receive Model | 13 |
| 2.1.2 | Linear System Model | 14 |
| 2.2 | Fading | 15 |
| 2.2.1 | Definition | 15 |
| 2.2.2 | Physical Parameters | 16 |
| 2.3 | Reflecting Wall | 17 |
| 2.3.1 | Simulation Overview | 17 |
| 2.3.2 | Simulation Results | 18 |
| 2.3.3 | MATLAB Graphical Simulation | 18 |
| 2.4 | Statistical Analysis of the Channel | 22 |
| 2.4.1 | Simulation Overview | 22 |
| 2.4.2 | Simulation Results | 23 |
| 2.4.3 | MATLAB Graphical Simulation | 24 |
| 3 | Antenna Beamforming in Multiuser Fading Channels | 31 |
| 3.1 | Preliminaries | 31 |
| 3.1.1 | Antenna Arrays | 31 |
| 3.1.2 | Downlink Fading Channel | 32 |
| 3.2 | Beamforming Using Dumb Antennas | 33 |

| | | |
|----------|---|-----------|
| 3.2.1 | Overview | 33 |
| 3.2.2 | Channel Representation | 34 |
| 3.2.3 | Beamforming Techniques | 34 |
| 3.3 | Dumb antennas and Multiuser Diversity | 36 |
| 3.3.1 | Multiuser Diversity | 38 |
| 3.3.2 | Assumptions | 39 |
| 3.3.3 | Rayleigh Fading | 40 |
| 3.3.4 | Rician Fading | 42 |
| 3.4 | MATLAB Graphical Simulation | 45 |
| 4 | Underlying Principles of OFDM | 51 |
| 4.1 | Eigenfunctions of LTI Systems | 51 |
| 4.2 | Frequency-selective Fading | 52 |
| 4.3 | Orthogonal Frequency Division Multiplexing (OFDM) | 53 |
| 4.3.1 | Motivation | 53 |
| 4.3.2 | Orthogonal Subcarriers | 53 |
| 4.3.3 | Finite Duration Sinusoids | 54 |
| 4.3.4 | Cyclic Prefix | 54 |
| 4.4 | MATLAB Graphical Simulation | 56 |
| 5 | Conclusion | 59 |
| 5.1 | Summary | 59 |
| 5.2 | Future Work | 60 |

List of Figures

| | | |
|------|--|----|
| 2-1 | Reflecting wall scenario | 17 |
| 2-2 | Reflecting wall simulation – Plot of the received signal at the MS | 19 |
| 2-3 | Reflecting wall – MATLAB graphical simulation | 21 |
| 2-4 | Statistical analysis scenario | 23 |
| 2-5 | Statistical analysis simulation – Mesh plot of $\Re\{H(f, t)\}$ | 24 |
| 2-6 | Statistical analysis simulation – Histogram of the pdf of $\Re\{H(f, t)\}$ | 25 |
| 2-7 | Statistical analysis simulation – Mesh plot of $\Im\{H(f, t)\}$ | 25 |
| 2-8 | Statistical analysis simulation – Histogram of the pdf of $\Im\{H(f, t)\}$ | 26 |
| 2-9 | Statistical analysis simulation – Mesh plot of $ H(f, t) $ | 26 |
| 2-10 | Statistical analysis simulation – Histogram of $ H(f, t) $ | 27 |
| 2-11 | Statistical analysis simulation – Histogram of the phase of fading | 27 |
| 2-12 | Statistical analysis – MATLAB graphical simulation: screenshot 1 | 29 |
| 2-13 | Statistical analysis – MATLAB graphical simulation: screenshot 2 | 30 |
| 3-1 | Uniform linear array | 32 |
| 3-2 | Beamforming using dumb antennas | 35 |
| 3-3 | ULA normalized beamforming pattern for 2 antennas | 37 |
| 3-4 | ULA normalized beamforming pattern for 4 antennas | 37 |
| 3-5 | ULA and random beamforming normalized beamforming patterns for 4 antennas | 38 |
| 3-6 | Rayleigh fading – Distribution of the overall chain gains | 41 |
| 3-7 | Rayleigh fading – Mean received power | 41 |
| 3-8 | Rayleigh fading – Overall channel gain of user 1 versus time | 42 |
| 3-9 | Rician fading – Distribution of the overall chain gains for $\kappa = 10$ | 44 |
| 3-10 | Rician fading – Distribution of the overall chain gains for $\kappa = 100$ | 44 |

| | |
|---|----|
| 3-11 Rician fading – Mean received power | 45 |
| 3-12 Rician fading – Overall channel gain of user 1 versus time | 46 |
| 3-13 Dumb antennas – MATLAB graphical simulation: screenshot 1 | 48 |
| 3-14 Dumb antennas – MATLAB graphical simulation: screenshot 2 | 49 |
| 3-15 Dumb antennas – MATLAB graphical simulation: screenshot 3 | 50 |
| | |
| 4-1 Discrete-time LTI system | 51 |
| 4-2 Tapped-delay line model | 53 |
| 4-3 Sinusoidal input and corresponding output | 55 |
| 4-4 Cyclic prefix addition | 55 |
| 4-5 OFDM – MATLAB graphical simulation: screenshot 1 | 57 |
| 4-6 OFDM – MATLAB graphical simulation: screenshot 2 | 58 |

Chapter 1

Introduction

1.1 Overview and Motivation

In undergraduate and graduate wireless communication courses, students are often introduced to the concepts of fading, wireless channels, multiuser environments and multi-antenna systems, together with the equations governing these systems and concepts. Often times, information theory is also brought into the picture, and students are frequently asked to deal with tedious derivations of the capacity of wireless channels.

The motivation of this thesis has been to bring out a simple yet efficient way to visualize wireless communication phenomena, and understand the underlying concepts and state-of-the-art technologies. The thesis presents a set of simulations for important models and algorithms in wireless communications. The simulations were implemented using the graphical user interface development environment (GUIDE) component of MATLAB. We chose MATLAB because it offers a wide range of tools to deal with complex equations, matrices and probabilistic models.

The simulations may be run in a typical classroom environment as a complement to slides or lecture notes, and are intended to help students understand important wireless communication concepts, tradeoffs, and standards. Moreover, the set of simulations could help the industry professionals review the key principles and visualize modern wireless technologies being simulated, without having to deal with mathematical complexities.

Of course, the wireless communication arena is vast and it would be difficult to present all key principles in a single manuscript. Nevertheless, we thought that the following important topics would be useful and appealing to a wide audience of students and engineers:

- **The wireless channel:** This is a fundamental topic in virtually every wireless communication course. Our interface simulates a simple two-path channel and covers the important physical parameters associated with any fading channel.
- **Statistical analysis of Rayleigh fading:** Rayleigh fading is a very common model for wireless channels. We simulated an intuitive scenario that proves the underlying probabilistic nature of the Rayleigh model.
- **Multiple antennas and multiuser environments:** These two topics constitute the bulk of many graduate courses in wireless communication. We coalesced the analysis into a single simulation that deals with dumb antennas, multiuser diversity and scheduling algorithms.
- **Orthogonal frequency division multiplexing (OFDM):** OFDM is a popular multicarrier technique that was recently incorporated into many wireless applications. Its digital implementation is quite complicated, but the basic idea – that sinusoids are eigenfunctions of LTI systems – is surprisingly simple and elegant. We implemented a graphical interface that abstracts this intuitive view of OFDM.

We hope that the graphical simulations that we have developed will help students and professionals understand key principles in wireless communication systems, without having to delve into mathematical details or analytical derivations.

1.2 Thesis Organization

The thesis proceeds in Chapter 2 with the analysis and simulation of a simple wireless channel. The more general Rayleigh model is described and simulated, as well. Chapter 3 investigates the use of dumb antenna in multiuser environments. The proportional fair algorithm is simulated in Rayleigh and Rician channels, using both ULA and random beamforming techniques. In Chapter 4 we explain the advantages of OFDM and illustrate the use of the cyclic prefix to combat intersymbol interference. Chapter 5 concludes the thesis.

Chapter 2

The Wireless Channel

In this chapter, we describe the physical aspects of a generic wireless communication channel. In Sec. 2.1 we look at a simple transmit-receive model and then derive a linear system model for wireless channels. In Sec. 2.2 we define the fading phenomenon and analyze its main parameters. In Sec. 2.3 we analyze and simulate a simple two-path wireless channel. Finally, in Sec. 2.4 we complete the description by coalescing the development into the well-known Rayleigh fading model, which we discuss and simulate as well.

2.1 Modeling of Wireless Channels

This section describes a simple modeling of wireless channels, and is primarily based on the analysis in [2].

2.1.1 Transmit-Receive Model

Consider a fixed antenna (base station) transmitting into free space. In the far field, assume that there is a receiving antenna (mobile station), at a location $\boldsymbol{\rho}(t) = (r(t), \theta, \phi)$,¹ moving away from the transmitting antenna. Hence, the electric field at the mobile station at time t , in response to a sinusoid $\exp(j2\pi ft)$ can be expressed as [2]

$$E(f, t, \boldsymbol{\rho}(t)) = \frac{F(\theta, \phi, f) \exp[j2\pi f(t - \frac{r(t)}{c})]}{r(t)}, \quad (2.1)$$

where $F(\theta, \phi, f)$ is the product of the antenna pattern functions of the transmit and

¹Here, t represents time, and $(r(t), \theta, \phi)$ are the spherical coordinates of the mobile station

receive antennas, and $c = 3 \times 10^8$ m/s is the speed of light.

2.1.2 Linear System Model

In the above scenario, the wireless channel has one direct path between the transmit and receive antennas, called the line of sight (LOS). In other more general situations, the wireless medium may or may not include a LOS component, and could then be described by a collection of I paths that usually result from reflection, scattering, shadowing, or other phenomena produced by the surroundings. Assuming that the pattern function $F(\cdot)$ does not depend on the frequency f , [2] expresses the overall response $y(t)$ to an input $\exp(j2\pi ft)$ as a direct generalization of Eq. (2.1), i.e.,

$$y(t) = \sum_{i=1}^I \frac{F_i(t) \exp[j2\pi f(t - \frac{r_i(t)}{c})]}{r_i(t)} \quad (2.2)$$

It is important to note that there are cases where the electric field does not attenuate as $1/r$, so it is more convenient to replace Eq. (2.2) with an expression that uses attenuation explicitly; we denote the complex attenuation on path i by $a_i(t)$.² We also define the time delay of path i as $\tau_i(t) = \frac{r_i(t)}{c}$. Hence, Eq. (2.2) may be rewritten as

$$y(t) = \sum_{i=1}^I a_i(t) \exp\{j2\pi f[t - \tau_i(t)]\} \quad (2.3)$$

If we factor out the input $\exp(j2\pi ft)$, then Eq. (2.3) becomes

$$y(t) = H(f, t) \exp(j2\pi ft), \quad (2.4)$$

where $H(f, t)$ is the system function of the linear time-variant (LTV) wireless system, and is defined as

$$H(f, t) = \sum_{i=1}^I a_i(t) \exp[-j2\pi f\tau_i(t)] \quad (2.5)$$

Let $h(\tau, t)$ be the inverse Fourier transform of $H(f, t)$, with time variable τ and parameter t . Then $h(\tau, t)$ is the channel impulse response of the LTV system, and can be expressed

² $a_i(t)$ is a complex-valued attenuation function for path i that takes into consideration both amplitude and phase changes caused the various wireless phenomena. In the case where the electric field decays as $1/r$, $a_i(t) = \frac{F_i(t)}{r_i(t)}$.

as [2, 5]

$$h(\tau, t) = \sum_{i=1}^I a_i(t) \delta[\tau - \tau_i(t)], \quad (2.6)$$

where $\delta(\cdot)$ is the Dirac delta function.

It can be shown that the response $y(t)$ to an input $x(t)$ is given by the convolution equation for LTV systems [2]:

$$y(t) = \int_{-\infty}^{\infty} h(\tau, t) x(t - \tau) d\tau \quad (2.7)$$

Substituting Eq. (2.6) into Eq. (2.7), we get

$$y(t) = \sum_{i=1}^I a_i(t) x[t - \tau_i(t)] \quad (2.8)$$

This says that the output signal can simply be described as the sum of attenuated and time-delayed versions of the input waveform.

2.2 Fading

2.2.1 Definition

The superposition of several signals at the receiver having different attenuations, delays and phase shifts, causes the distortion of the transmitted signal. This phenomenon is called fading, and can be understood more fundamentally by considering again the case where a sender is transmitting a sinusoid $\exp(j2\pi ft)$. By expressing $H(f, t)$ in the phasor notation, i.e. $|H(f, t)| \exp[j\angle H(f, t)]$, Eq. (2.4) becomes [2]

$$y(t) = |H(f, t)| \exp\{j[2\pi ft + \angle H(f, t)]\} \quad (2.9)$$

We further consider the real and imaginary components of $y(t)$, which are the output responses to $\cos(2\pi ft)$ and $\sin(2\pi ft)$, respectively, i.e.

$$\Re\{y(t)\} = |H(f, t)| \cos[2\pi ft + \angle H(f, t)] \quad (2.10)$$

$$\text{and } \Im\{y(t)\} = |H(f, t)| \sin[2\pi ft + \angle H(f, t)] \quad (2.11)$$

We can see that both real and imaginary responses vary at approximately the frequency f , inside the slowly varying envelope $\pm|H(f, t)|$ [2]. Therefore, in this simple model, we may define the fading amplitude as $|H(f, t)|$, and the fading phase as $\angle H(f, t)$.

2.2.2 Physical Parameters

Several parameters are used to characterize fading. Those include the Doppler spread, the coherence time, the delay spread and the coherence bandwidth.

The Doppler effect says that if for path i , the receiver is moving with a relative velocity v , and an angle of arrival ϑ_i , then the transmitted signal's frequency f is not the same at the receiver, but differs by the Doppler shift [1]

$$\mathcal{D}_i = -f \frac{v}{c} \cos \vartheta_i \quad (2.12)$$

If the wireless channel has I paths between the sender and receiver, then the Doppler spread \mathcal{D}_s is defined as the difference between the largest and smallest Doppler shift over all paths [2], for $i = 1, 2, \dots, I$. That is,

$$\mathcal{D}_s = \max_i \mathcal{D}_i - \min_i \mathcal{D}_i \quad (2.13)$$

A closely related parameter is the coherence time \mathcal{T}_c of the channel, which approximates the typical time interval for the fading the change significantly. Mathematically, the coherence time can be expressed as [2]

$$\mathcal{T}_c = \frac{1}{2\mathcal{D}_s} \quad (2.14)$$

Another important parameter is the delay spread \mathcal{T}_d of the channel, which is the difference between the longest and shortest time delay at some given time t , over all paths, i.e. [2]

$$\mathcal{T}_d = \max_i \tau_i(t) - \min_i \tau_i(t) \quad (2.15)$$

Finally, the coherence bandwidth \mathcal{W}_c of the channel approximates how much the frequency of the system must be changed in order for a deeply faded channel to become unfaded, and vice versa. It is defined as [2]

$$\mathcal{W}_c = \frac{1}{2T_d} \quad (2.16)$$

2.3 Reflecting Wall

The purpose of this section is to highlight the key parameters of Sec. 2.2 using a simple reflection example. The idea of the simulation is primarily based on the reflecting wall example of [5].

2.3.1 Simulation Overview

Consider Fig. 2-1 in which there is a fixed antenna sending a sinusoid $\exp(j2\pi ft)$ in free space, and a mobile station (MS) moving away from the antenna at a constant velocity v . At $t = 0$, the MS is at distance r_0 from the transmitting antenna; furthermore, there is a large and perfectly reflecting wall at a fixed distance d from the antenna.

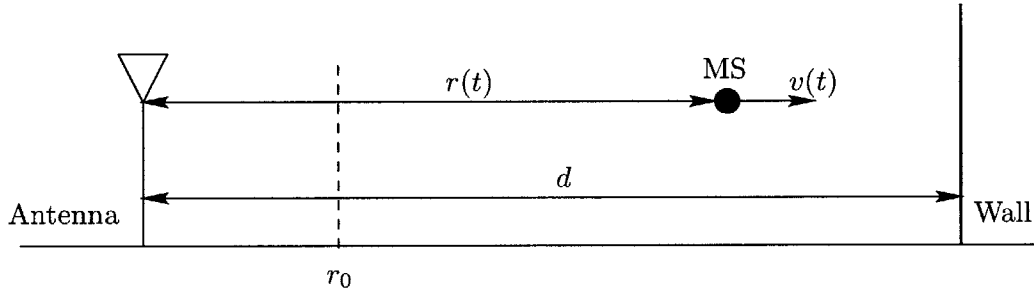


Figure 2-1: Reflecting wall scenario

Two signals superpose at the MS as it moves: the signal of the direct path from the transmitting antenna, having a time delay of τ_1 , and the signal of the reflected path from the wall, having a delay of τ_2 . Assuming that the MS antenna pattern is identical for both paths, and noting the phase reversal for the reflected path, we can write the path attenuations as [5]

$$a_1(t) = \frac{F}{r_0 + vt} \quad a_2(t) = -\frac{F}{2d - (r_0 + vt)}, \quad (2.17)$$

and the time delays as

$$\tau_1(t) = \frac{r_0 + vt}{c} \quad \tau_2(t) = \frac{2d - (r_0 + vt)}{c}, \quad (2.18)$$

where F is the (constant) product of the pattern functions of the sending antenna and the MS. It follows that the instantaneous delay spread can be written as: $\mathcal{T}_d = |\tau_1(t) - \tau_2(t)| = \left| \frac{2(r_0 + vt - 2d)}{c} \right|$.

By substituting Eqs. (2.17) and (2.18) into Eq. (2.3), we get the instantaneous response $y(t)$ at the MS, i.e.

$$y(t) = \frac{F \exp\{j2\pi f[(1 - \frac{v}{c})t - \frac{r_0}{c}]\}}{r_0 + vt} - \frac{F \exp\{j2\pi f[(1 + \frac{v}{c})t - \frac{r_0 - 2d}{c}]\}}{2d - r_0 - vt} \quad (2.19)$$

We can see that the direct response is a sinusoid of frequency $f(1 - \frac{v}{c})$, whereas the reflected response is a sinusoid of frequency $f(1 + \frac{v}{c})$. Therefore, the Doppler shifts for the 2 paths are $\mathcal{D}_1 = -f\frac{v}{c}$ and $\mathcal{D}_2 = f\frac{v}{c}$, respectively, which means that the Doppler spread is $\mathcal{D}_s = 2f\frac{v}{c}$.

2.3.2 Simulation Results

The parameters used are: $f = 900$ MHz, $d = 2.5$ km, $r_0 = 2.25$ km, $v = 20$ m/s and $F = 1$, which means that $\mathcal{D}_s = 120$ Hz and $\mathcal{T}_c \approx 4.2$ ms. Fig. 2-2 shows the response at the receiver, as well as the fading envelope, during the approximate time interval (8, 40) ms.

As we can see, the response can be approximated by a sinusoid of frequency f , with a varying fading envelope whose peaks and valleys alternate every \mathcal{T}_c seconds. Indeed, the MS is much closer to the reflector than to the transmitter, which means that the attenuations from both paths are approximately equal [5]. In this case, the received signal can be approximated by a product of two sinusoids of frequencies f and $\mathcal{D}_s/2$ respectively [5], which explains why the response has a time-varying envelope.

2.3.3 MATLAB Graphical Simulation

Fig. 2-3 shows a screenshot of our MATLAB simulation of the reflecting wall scenario. The interface was developed in the GUIDE component of MATLAB, and comprises five main parts:

- **Simulation parameters:** This panel contains five important parameters that the user can change before running the simulation. These parameters are the carrier frequency f , the velocity v of the MS, the distance d between the transmitter and the

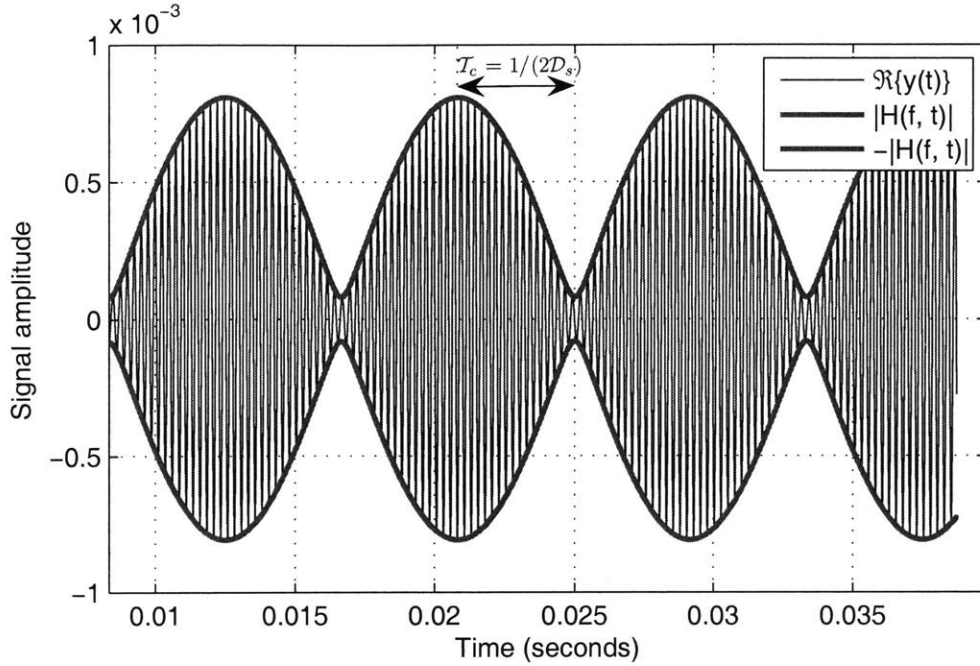


Figure 2-2: Plot of the received signal and the fading envelope for $t \in (8, 40)$ ms. The response varies at the frequency f between the time-varying fading envelope. The coherence time \mathcal{T}_c is the interval over which the fading changes significantly

wall, the initial distance r_0 between the transmitter and receiver and the product of antenna gains F .

- **Animation panel:** This panel contains an illustration of the reflecting wall scenario. The mobile station is represented by a small filled circle that moves towards the reflector while the animation is taking place.
- **Control panel:** This part of the interface has three buttons that allow the user to control the running simulation. The Start Animation button uses the saved parameters to start the simulation. The Pause Animation button pauses the simulation at any time, and Resume Animation resumes it wherever it stopped.
- **Statistics panel:** Once the simulation parameters get saved, this panel displays the numerical values of the Doppler spread and the coherence time.
- **Received signal figure:** The received signal at the mobile station is plotted versus time, as the simulation is taking place. The thick lines around the response represent the time-varying fading envelope.

The user could observe the effect of each parameter by separately changing it while holding all the others constant. An interesting simulation would be to test how the response at the receiver looks when the MS is much closer to the transmitter than to the wall ($r_0 \ll d$). In this case, the reflected signal's amplitude will be negligible, and the effect of fading will not be very obvious.

The users may restart a new simulation by going to the Options menu, and selecting Reset. This will enable them to input new parameters and observe the changes on the received signal and fading envelope.

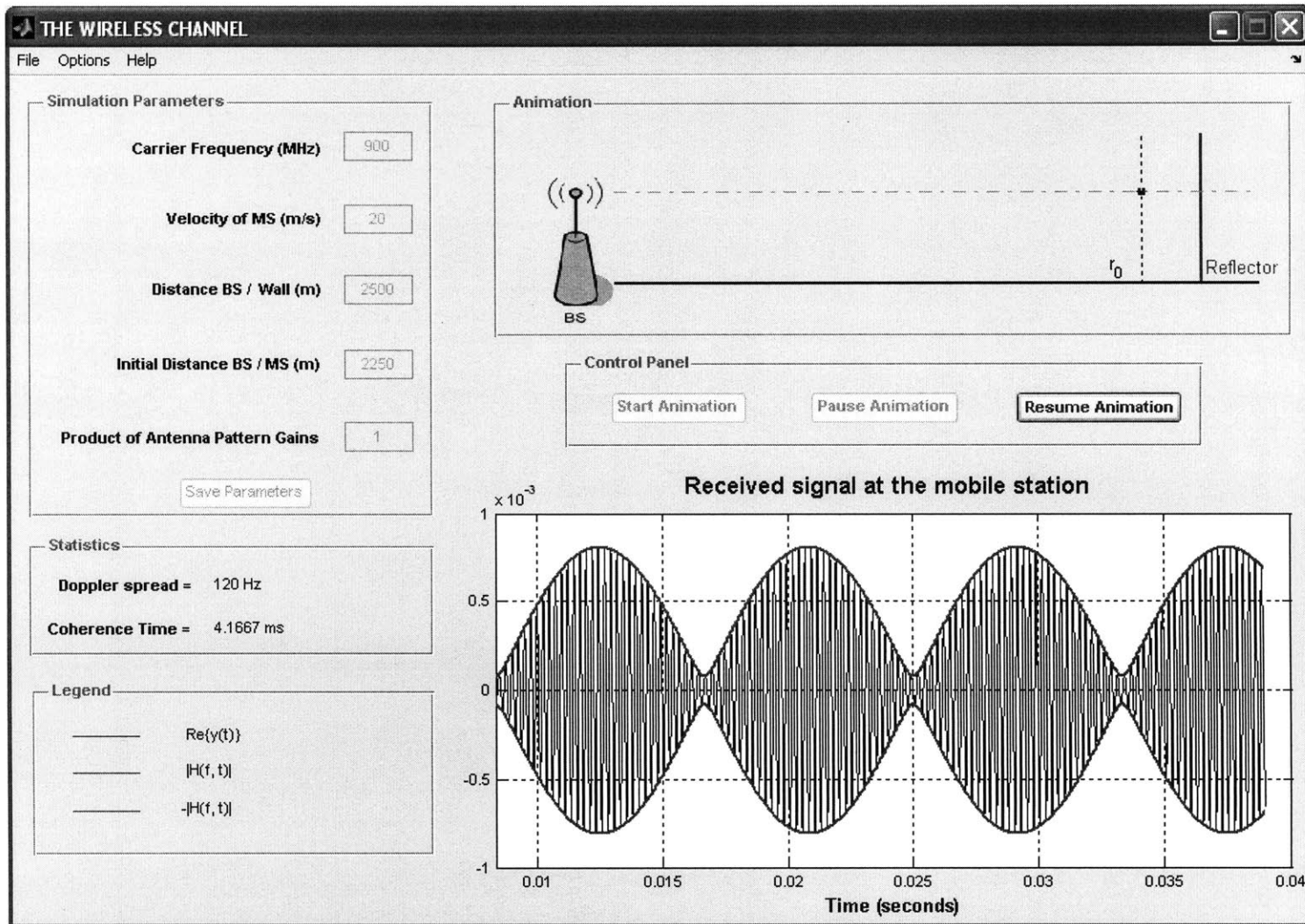


Figure 2-3: Reflecting wall – MATLAB graphical simulation. The received signal and the fading envelope are plotted dynamically on the figure while the MS is moving towards the reflector in the Animation panel

2.4 Statistical Analysis of the Channel

In situations where the received signal consists of several paths, the derivation of the response at the receiver becomes tedious. In that case, it is more convenient to model the channel statistically, i.e. to consider a probabilistic model for fading.

One of the widely used statistical models is the Rayleigh fading model, where the fading is modeled as a complex Gaussian random variable, whose real and imaginary components are zero-mean Gaussian random variables, and whose magnitude is Rayleigh-distributed.³ This model applies well in scenarios where the number of paths I is relatively large. By the central limit theorem, both real and imaginary parts of the fading are the sum of several independent components, and thus will approximately be distributed as zero-mean Gaussian variables, for a sufficiently large I . Mathematically, the magnitude of such fading is Rayleigh distributed, and it can be shown that the phase is uniformly distributed [5] over $[-\pi, \pi]$. However, even though this model is a very good approximation in several practical cases, it is important to mention that it loses its validity when I is not large enough, or when there is a dominant (LOS) path between the transmitter and receiver [4].

2.4.1 Simulation Overview

We now describe the simulation of the Rayleigh fading channel using the simple case scenario of Fig. 2-4. This simulation is based on an example found in [4]. A transmitter is sending a sinusoid $\exp(j2\pi ft)$ in free space, and in the far field, there is a mobile station moving over a square region \mathcal{A} . There are I reflectors (scatterers) between the BS and the MS, which signifies that the MS is receiving I attenuated and time-delayed copies of the original signal. Furthermore, we assume that there is no LOS between the sender and receiver, and that the reflectors are distributed in a quasi uniform fashion around the area \mathcal{A} .

We denote by $\boldsymbol{\rho} = x\mathbf{i} + y\mathbf{j}$ the instantaneous location vector of the MS,⁴ and by $\boldsymbol{\kappa}_i$ the wave propagation unit vector for path i . If ϑ_i is the angle of arrival of path i with respect to the y -axis, then the projection of the propagation vector onto the location vector can be

³The density of a Rayleigh-distributed random variable X is given by: $f_X(x) = \frac{x}{\sigma^2} \exp(-\frac{x^2}{2\sigma^2})$, $x \geq 0$.

⁴ \mathbf{i} and \mathbf{j} are the unit vectors of the x and y axes, respectively.

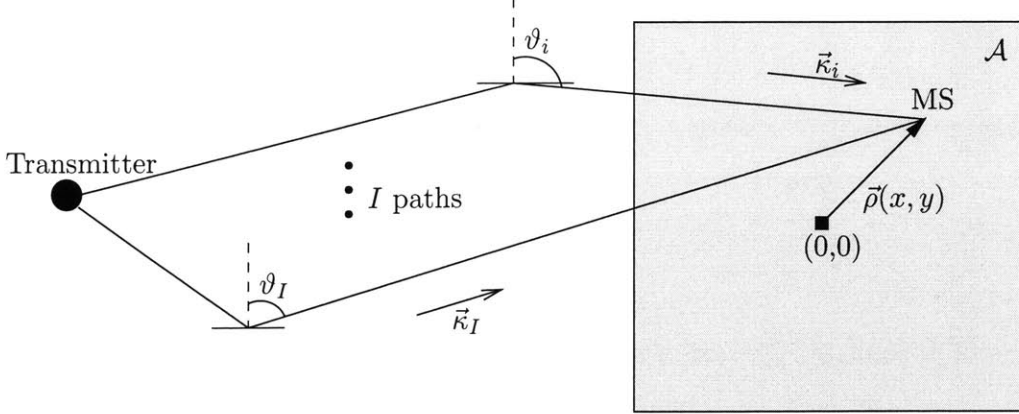


Figure 2-4: Statistical analysis scenario

written as

$$\begin{aligned}
 \langle \boldsymbol{\kappa}, \boldsymbol{\rho} \rangle &= \langle \boldsymbol{\kappa}, x\mathbf{i} + y\mathbf{j} \rangle \\
 &= \langle \boldsymbol{\kappa}, x\mathbf{i} \rangle + \langle \boldsymbol{\kappa}, y\mathbf{j} \rangle \\
 &= x \sin \vartheta_i + y \cos \vartheta_i
 \end{aligned} \tag{2.20}$$

Since we are interested in analyzing the fading $H(f, t)$ statistically, we may, without loss of generality, consider a particular time instant, say $t = 0$. We denote the attenuation and path delay at $t = 0$ as a_i and τ_i , respectively. Assuming that path i has a phase of φ_i , then a_i can be written as $|a_i| \exp(j\varphi_i)$. By writing the path delay as $\tau_i = \frac{\langle \boldsymbol{\kappa}, \boldsymbol{\rho} \rangle}{c}$, and by substituting Eq. (2.20) into Eq. (2.5), we get

$$H(f, t = 0) = \sum_{i=1}^I |a_i| \exp(j\varphi_i) \exp \left[-j \frac{2\pi f}{c} (x \sin \vartheta_i + y \cos \vartheta_i) \right] \tag{2.21}$$

We claimed earlier that for I large enough, both real and imaginary components of H should be normally distributed, and that its magnitude and phase should be Rayleigh- and uniformly-distributed, respectively. These findings were confirmed by our MATLAB simulations, as we will see next.

2.4.2 Simulation Results

The parameters used are: $I = 12$ paths, $f = 900$ MHz, and $\mathcal{A} = \{x \in [-6, 6] \text{ m} ; y \in [-6, 6] \text{ m}\}$. Furthermore, the angles of arrivals are chosen to be approximately uniform around \mathcal{A} ,

and the path attenuations are selected to be $|a_i| \sim \mathcal{N}(\mu = 1, \sigma^2 = 0.09)$.

In Fig. 2-5 through 2-11, we plot the fading over \mathcal{A} and draw the following conclusions:

- Fig. 2-5 through 2-8 confirm our analysis that both real and imaginary components of fading are approximately zero-mean Gaussian random variables.
- Fig. 2-9 and 2-10 show that the magnitude of fading is nearly Rayleigh distributed, which directly follows from the normality of both constituents of the complex fading variable.
- Finally, Fig. 2-11 confirms that the phase of fading is roughly uniformly distributed over the interval $[-\pi, \pi]$, again corroborating our earlier discussion.

These observations thus justify the nomenclature “Rayleigh fading” when the number of paths in the channel is large enough, and when the reflectors in the medium are approximately uniformly distributed around the receiving antenna.

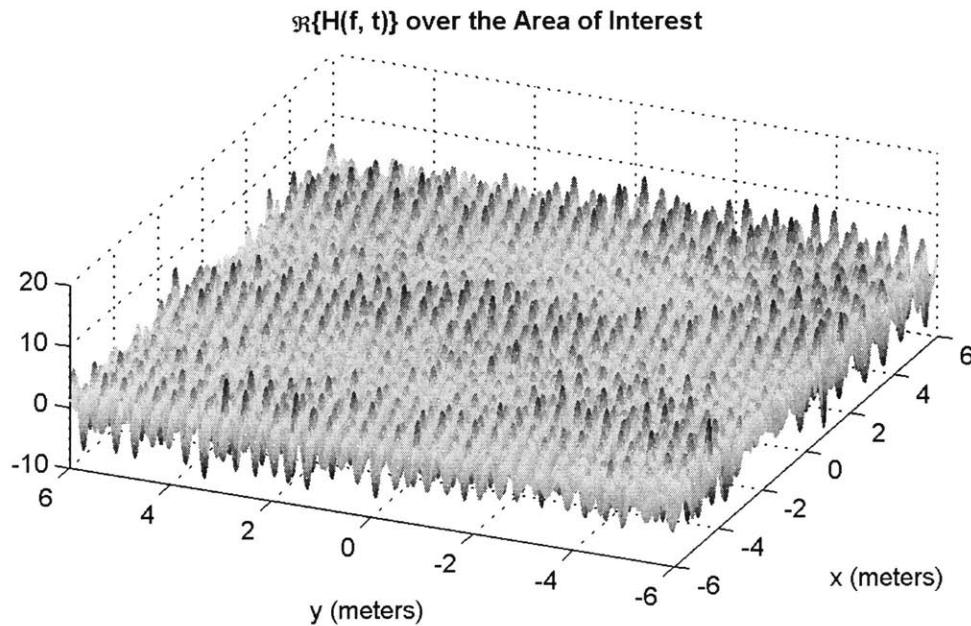


Figure 2-5: Mesh plot of $\Re\{H(f, t)\}$ over \mathcal{A} .

2.4.3 MATLAB Graphical Simulation

Fig. 2-12 and 2-13 show two screenshots of our MATLAB simulation of the statistical analysis scenario. The interface displays a small paragraph describing the statistical analysis

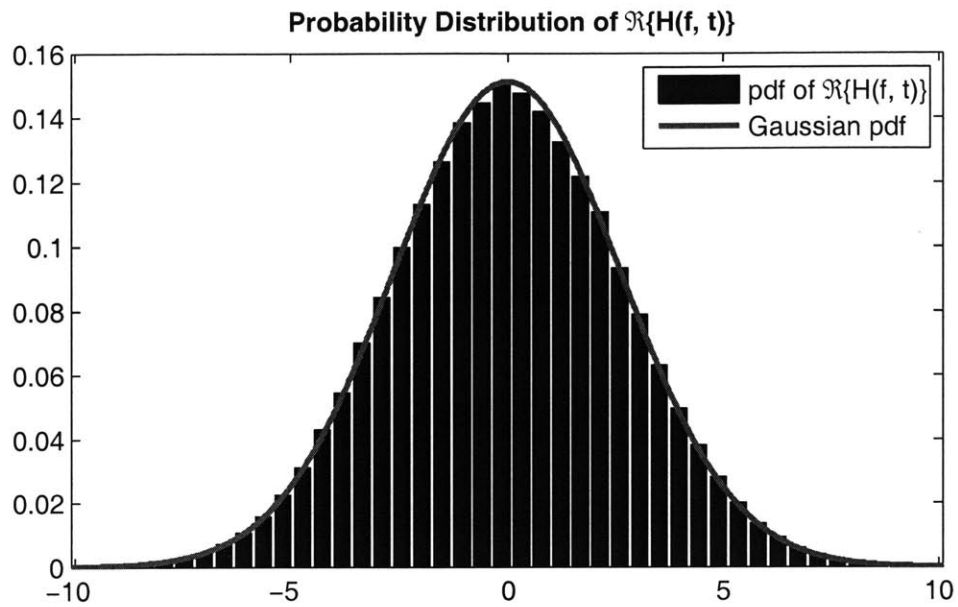


Figure 2-6: Histogram of the pdf of $\Re\{H(f, t)\}$. The red curve is the fitted zero-mean Gaussian pdf

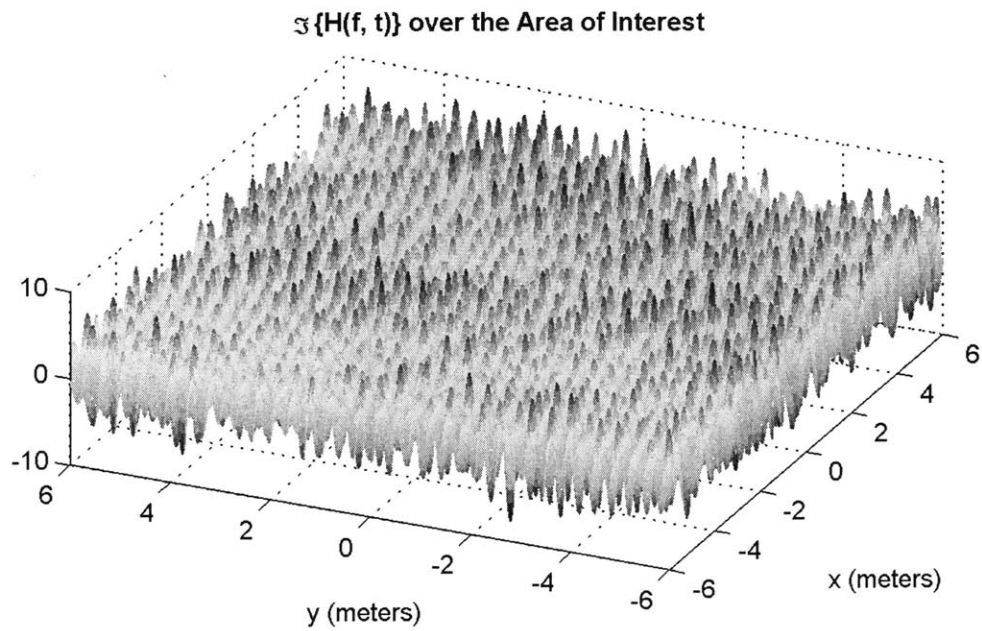


Figure 2-7: Mesh plot of $\Im\{H(f, t)\}$ over \mathcal{A}

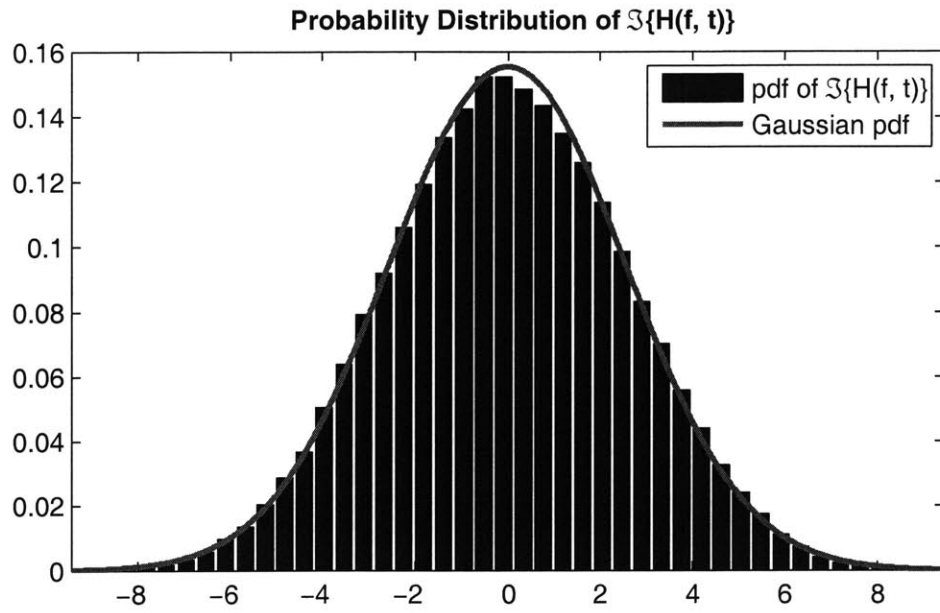


Figure 2-8: Histogram of the pdf of $\mathfrak{S}\{H(f, t)\}$. The thick curve is the fitted zero-mean Gaussian pdf

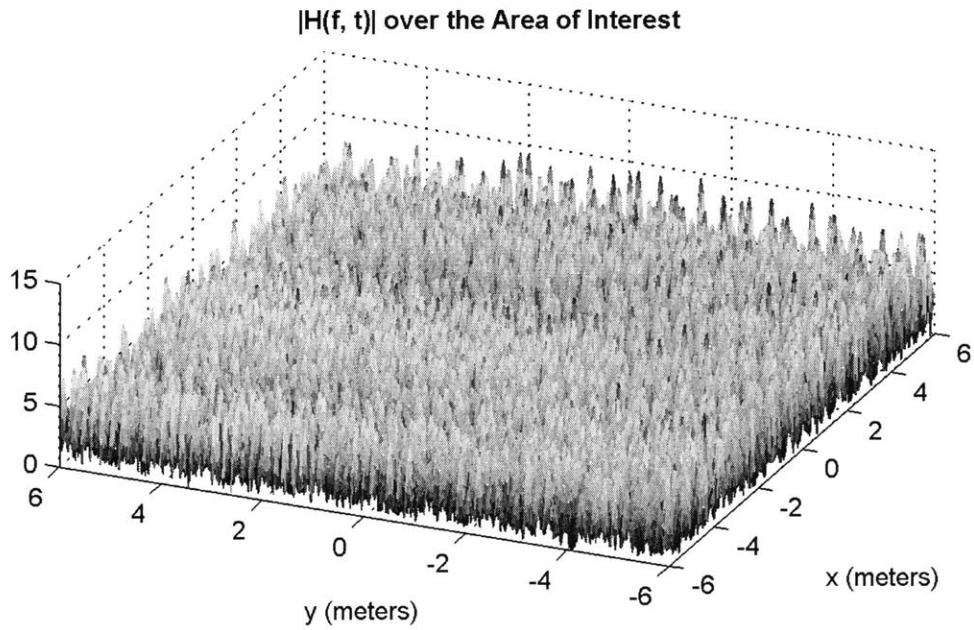


Figure 2-9: Mesh plot of $|H(f, t)|$ over \mathcal{A}

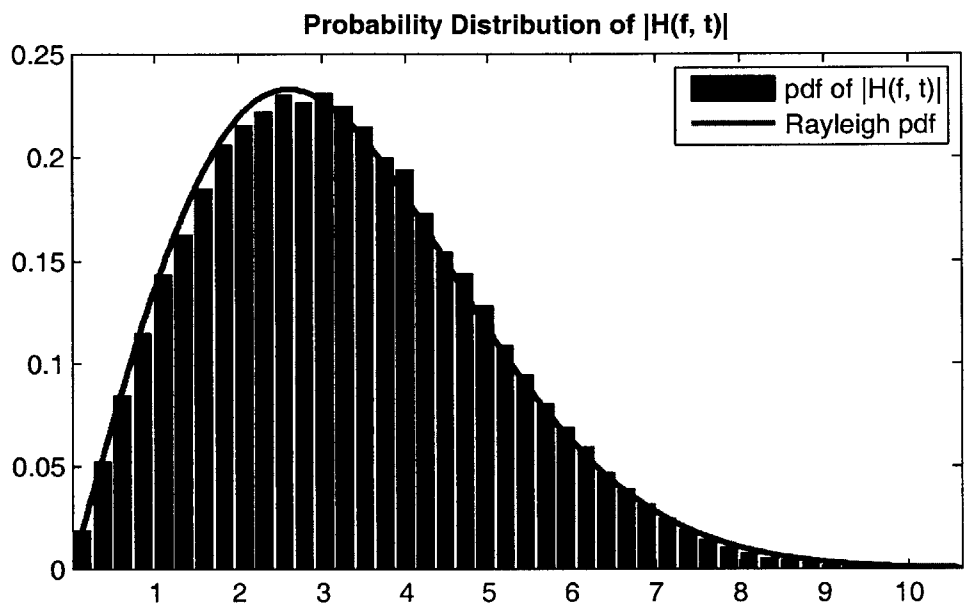


Figure 2-10: Histogram of the pdf of $|H(f, t)|$. The thick curve is the fitted Rayleigh pdf

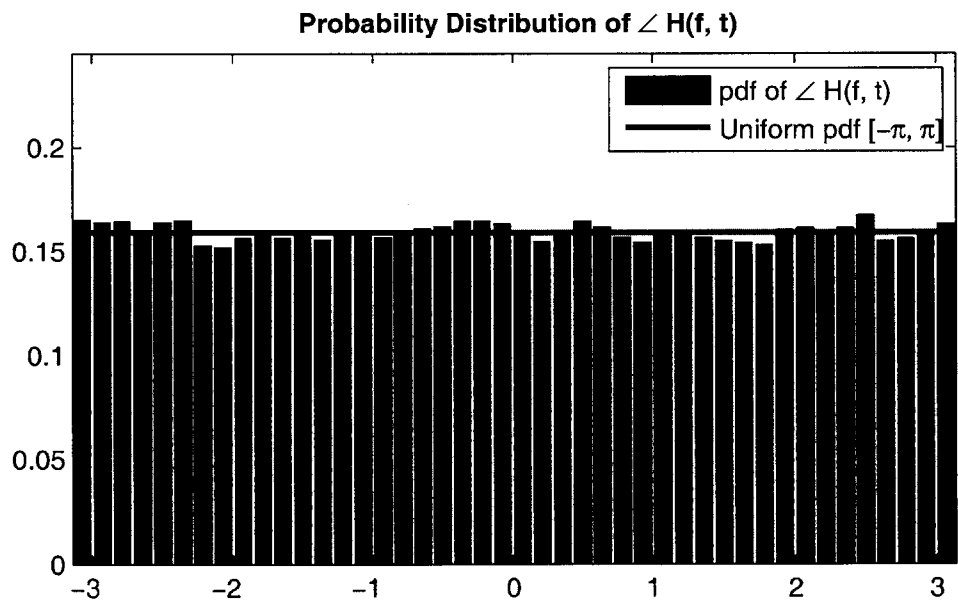


Figure 2-11: Histogram of the pdf of the phase of $H(f, t)$. The thick curve is the uniform pdf over $[-\pi, \pi]$

setup. After pressing the Simulate Rayleigh Fading button, the simulation parameters will be displayed, and these include:

- **Number of paths:** the number I of multipath components due to reflection or scattering.
- **Signal frequency:** the frequency f of the sinusoidal input.
- **Area of interest:** the square area \mathcal{A} in which the mobile station is moving.
- **Angles of arrival:** these are the angles at which the different reflected signals arrive at the mobile station. Note that these angles are approximately uniformly distributed around the region \mathcal{A} .
- **Path attenuations:** the attenuation of each of the I paths. These are normally distributed with mean $\mu = 1$ and a small variance, in order to prevent any path's signal from dominating the others.
- **Path phases:** the randomly generated phases of each path's attenuation.

The “Next” ($>>$) button allows the user to view the next plot, and the “Previous” ($<<$) button displays the previous plot. The plots that are being generated are the same as the ones we showed in Fig. 2-5 through 2-11. For example, Fig. 2-13 shows the histogram of the imaginary component of fading, along with the fitted Gaussian distribution. The user may restart a new simulation by going to the Options menu, and selecting Reset.

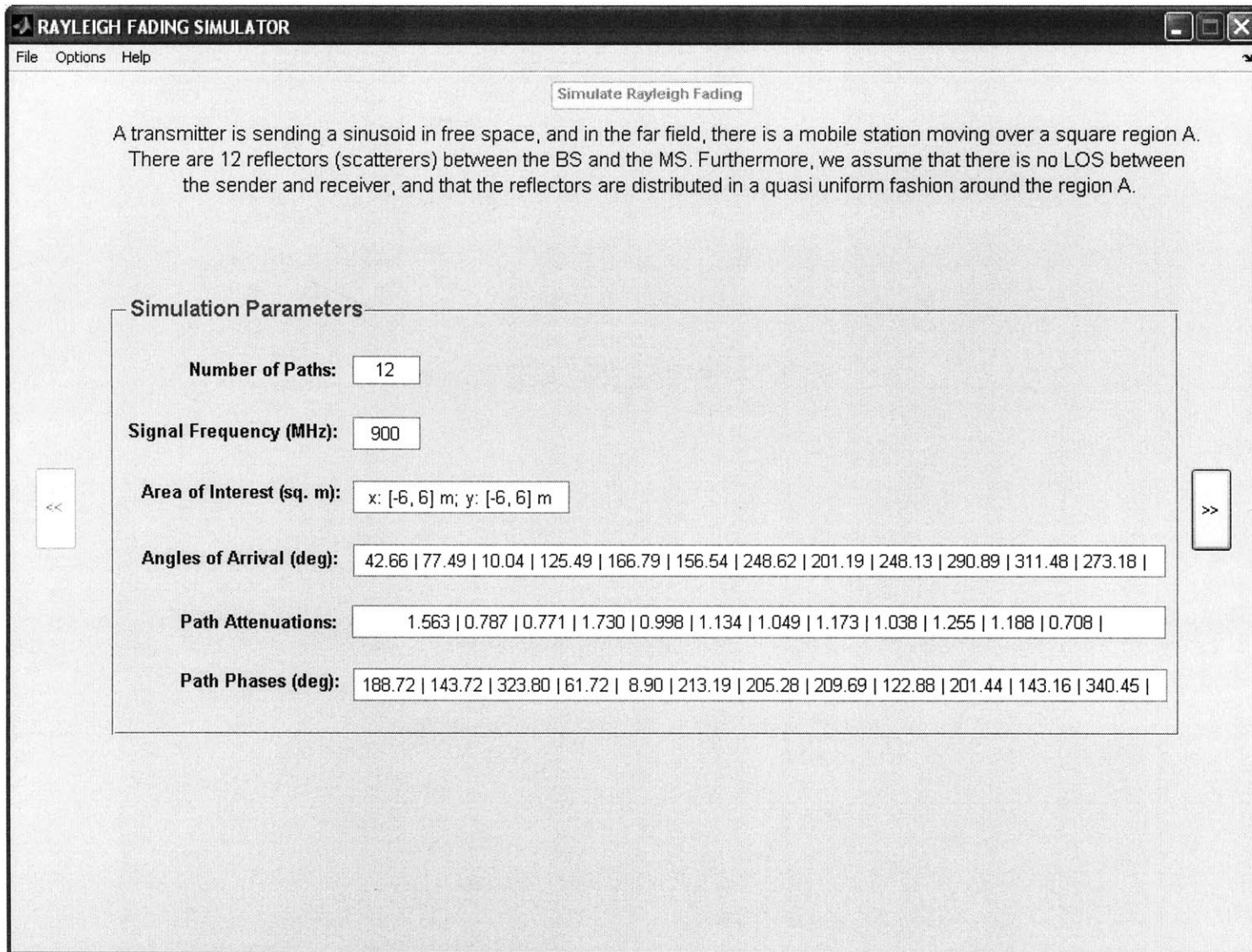


Figure 2-12: Statistical analysis - MATLAB graphical simulation. After the simulation parameters get displayed, the user can visualize the fading plots and statistics

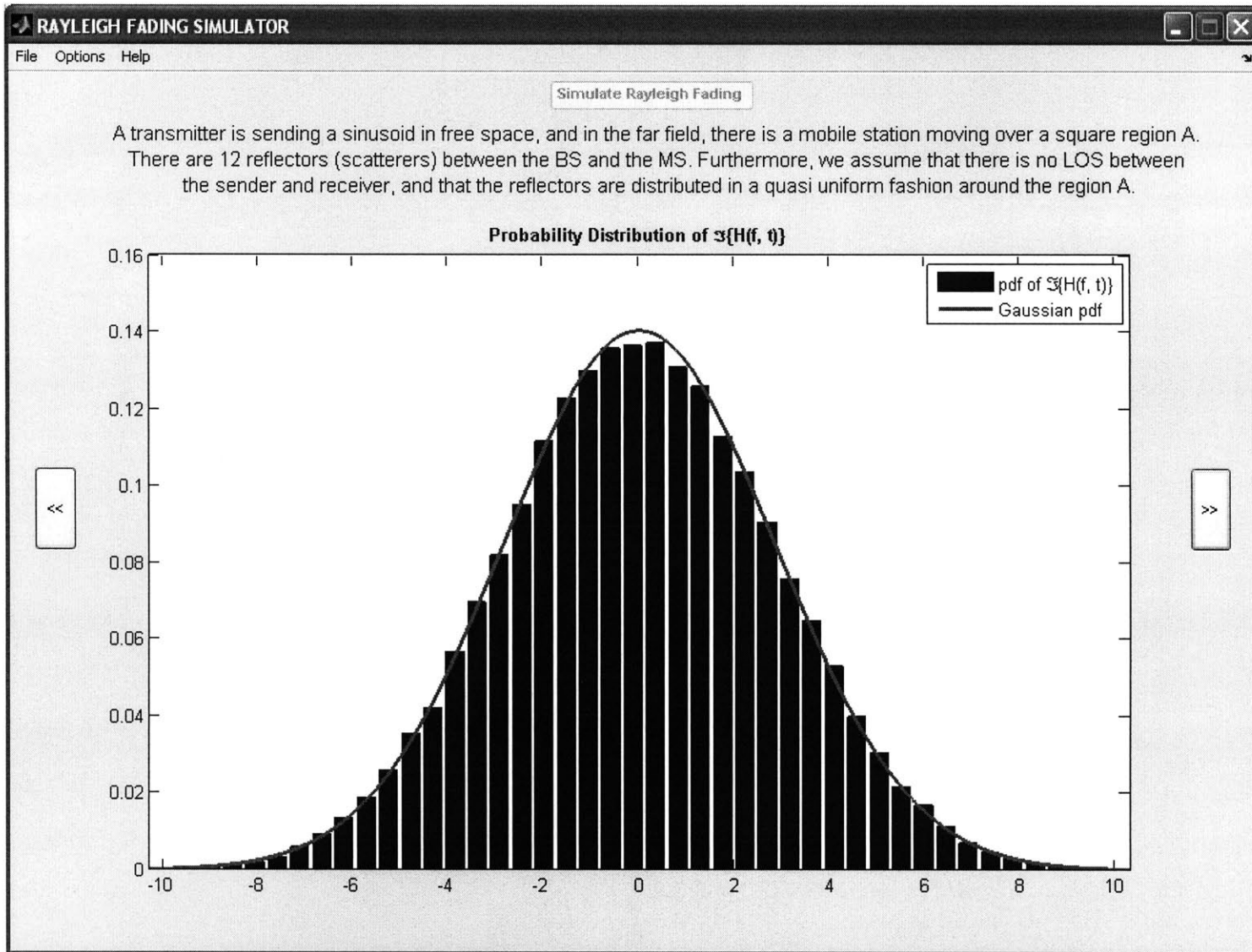


Figure 2-13: Statistical analysis - MATLAB graphical simulation. The pdf of $\mathfrak{S}\{H(f, t)\}$ is one of the 7 plots that could be displayed. The other plots can be viewed by pressing \gg or \ll

Chapter 3

Antenna Beamforming in Multiuser Fading Channels

In this chapter, we address the issue of antenna beamforming in a multiuser faded environment. In Sec. 3.1 we look at linear antenna arrays and describe a generic downlink fading channel. In Sec. 3.2 we give an overview of beamforming and discuss beamforming techniques using dumb antennas. In Sec. 3.3 we investigate the relationship between dumb antennas and multiuser diversity, and analyze it in both multiuser Rayleigh and Rician fast-faded environments. Finally, in Sec. 3.4, we describe our MATLAB simulation in detail.

3.1 Preliminaries

3.1.1 Antenna Arrays

In general, single-element linear antennas have low directivity and their main beams point to fixed directions [1]. Directivity is an important property of antennas, and can be defined as the ratio of the maximum radiation intensity in a particular direction to the average intensity radiated in all directions [1].

An antenna array denotes the arrangement of several antennas into a specific configuration in order to produce a better directivity at certain locations in space. Often times, these antennas are coupled to a common source, and the currents feeding them usually have varying relative amplitudes and phases.

Uniform Linear Arrays

In a uniform linear array (ULA), two or more equally spaced antennas are fed with signals having the same amplitude and a uniform progressive phase shift between them. We consider a linear array with N_t antennas placed along a horizontal line, and we denote by d the distance between consecutive array elements. The antenna spacing d is usually expressed in terms of the carrier wavelength λ . In the remainder of the chapter, we assume that $d = \frac{\lambda}{2}$.

As shown in Fig. (3-1), the antennas are numbered sequentially from 1 to N_t , so that the progressive phase shift mechanism assigns a phase of $(n-1)\xi$ to the n^{th} antenna, where $n = 1, 2, \dots, N_t$.

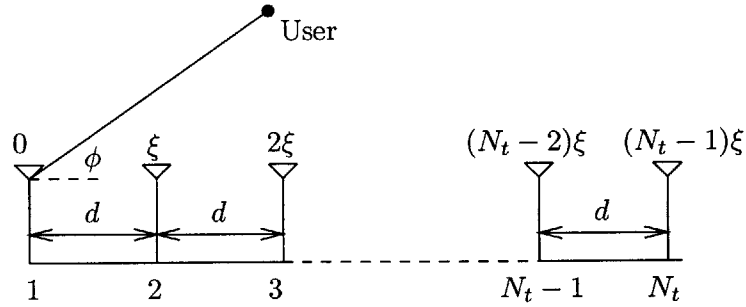


Figure 3-1: A uniform linear array with N_t antennas placed along the horizontal axis, transmitting to a user in the far field. The signal in each antenna leads the previous one's by a constant phase shift ξ

The variation of the intensity of radiation of the antenna array as a function of the departure angle ϕ is often called the array factor. For a user located in the far field, the normalized array factor can be expressed as [1]

$$|A(\theta)| = \frac{1}{N_t} |1 + e^{j\theta} + e^{j2\theta} + \dots + e^{j(N_t-1)\theta}|, \quad (3.1)$$

where

$$\theta = \frac{2\pi}{\lambda} d \cos \phi + \xi \quad (3.2)$$

3.1.2 Downlink Fading Channel

The simplest model of a downlink communication channel features a single transmitter (with one antenna) sending information to several users. For a downlink flat-fading channel with K users, and time index m , the fading process of user k is denoted by $\{h_k[m]\}$. There is a

power constraint $P = 1$ on the input signal $x[m]$, and the noise process of user k , $\{z_k[m]\}$, is assumed to be white Gaussian with mean 0 and variance N_0 , i.e. $z_k[m] \sim \mathcal{CN}(0, N_0)$. If user k receives the signal y_k at time m , then the downlink fading channel can be represented generically by the following model:

$$y_k[m] = h_k[m]x[m] + z_k[m] \quad k = 1, 2, \dots, K. \quad (3.3)$$

In many situations, several antennas are placed at the transmitter (base station), say N_t . In this case, the channel between the transmitter and user k is often called a multiple input single output (MISO) channel. Assuming that the input at time m is now $\mathbf{x}[m] = (x_1[m], x_2[m], \dots, x_{N_t}[m])^t$, and denoting the fading realization between antenna n and user k by $h_{n,k}[m]$, the channel can then be modeled as

$$y_k[m] = \mathbf{h}_k[m]^\dagger \mathbf{x}[m] + z_k[m] \quad k = 1, 2, \dots, K, \quad (3.4)$$

where $\mathbf{h}_k[m]^\dagger = (h_{1,k}[m], \dots, h_{N_t,k}[m])$ is the fading vector from the antenna array to user k .

3.2 Beamforming Using Dumb Antennas

3.2.1 Overview

Beamforming is a technique used to direct the beam of an antenna array in such a way to have more power received in certain directions. In the remainder of the chapter, we investigate the use of *dumb antennas* to induce beamforming, an area which was investigated by Viswanath et al. in [6].

Unlike transmit beamforming techniques, dumb antennas do not know the location of the users and need not measure their individual channel gains. Each user k only feeds back its own received signal-to-noise ratio (SNR) to the base station; the latter employs a scheduling algorithm that transmits data to a specific user in each time slot [6].

3.2.2 Channel Representation

As shown in Fig. (3-2), the scheme proposed in [6] transmits $\mathbf{x}[m] = \mathbf{w}_k[m]\tilde{x}[m]$ to user k at time m , where $\mathbf{w}_k[m]$ is the transmit *weight vector* of user k , and is defined as

$$\mathbf{w}_k[m] = \begin{bmatrix} \sqrt{\alpha_1[m]}e^{j\psi_{1,k}[m]} \\ \sqrt{\alpha_2[m]}e^{j\psi_{2,k}[m]} \\ \vdots \\ \sqrt{\alpha_{N_t}[m]}e^{j\psi_{N_t,k}[m]} \end{bmatrix} \quad (3.5)$$

As we will see shortly, the phases $\psi_{n,k}$ could be chosen randomly and independently (random beamforming), or could actually represent the phases of a uniform linear array. In either case, the power coefficients $\alpha_n[m]$ are chosen in such a way to preserve the total transmit power at time m , i.e. $\sum_{n=1}^{N_t} \alpha_n[m] = 1$.

It follows that the received signal for user k at time m is given by

$$y_k[m] = (\mathbf{h}_k[m]^\dagger \mathbf{w}_k[m])\tilde{x}[m] + z_k[m] \quad k = 1, 2, \dots, K \quad (3.6)$$

The *overall channel gain* of user k is the equivalent channel realization seen by user k after multiplying the fading coefficients by the weight vector, and is defined as $\mathbf{g}_k[m] := \mathbf{h}_k[m]^\dagger \mathbf{w}_k[m]$.

3.2.3 Beamforming Techniques

The time-varying attenuations and phases, $\alpha_n[m]$ and $\psi_{n,k}[m]$, could be chosen in various ways, thus producing different weight vectors. In this section, we describe two beamforming techniques and in subsequent sections, we compare their performance in fast fading environments.

Uniform Linear Beamforming

The ULA described in § 3.1.1 is an interesting example of dumb antennas. If we assume, here again, that the transmitter knows neither the users' locations nor their channel gains, fluctuations in the channel can be induced simply by changing the progressive phase shift ξ . We coin this technique *uniform linear beamforming* to imply that the beam is produced

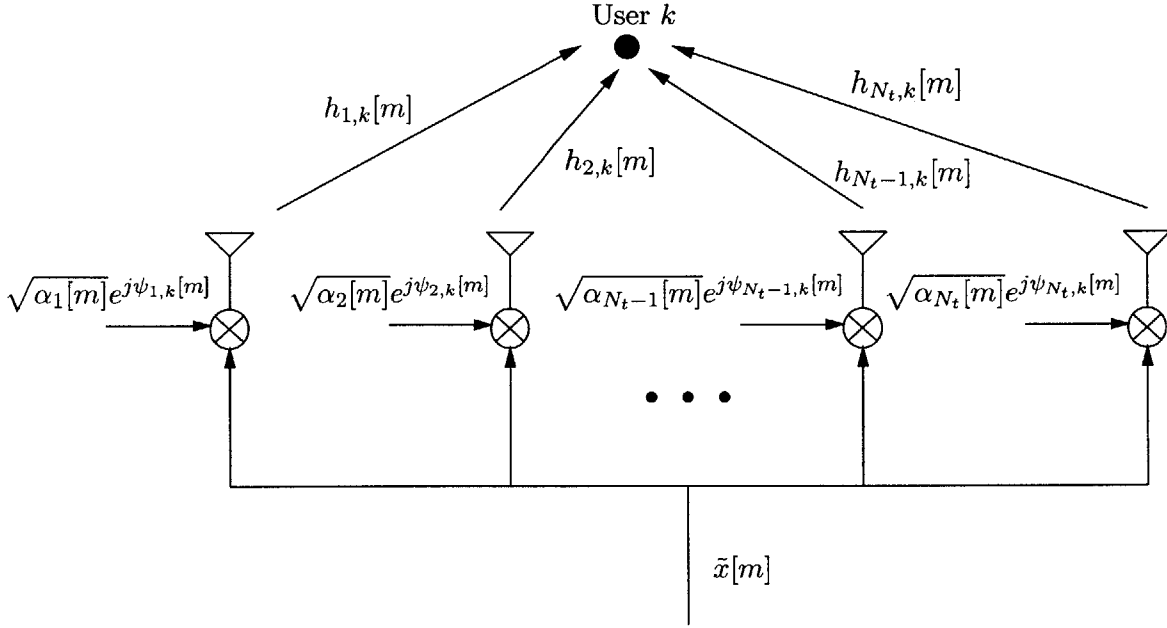


Figure 3-2: Beamforming using dumb antennas: the signal sent by each antenna is a modified version of the scalar $\tilde{x}[m]$, with time-varying powers and phases

by a ULA.

By conveniently choosing the phase shift ξ , the main beam can be steered to a specific *steering angle* ϕ_S in the plane. Consequently, at each time m , the transmitter randomly picks a phase shift ξ uniformly distributed between 0 and 2π , independently of previous time slots. It can be shown that the steering angle ϕ_S is related to the phase shift ξ by $\phi_S = \cos^{-1}(-\frac{\lambda}{2\pi d} \cdot \xi)$.

By using Eq. (3.2), it follows that the instantaneous phase of user k due to the signal from the n^{th} antenna is given by

$$\begin{aligned} \psi_{n,k} &= (n-1) \left(\frac{2\pi}{\lambda} d \cos \phi_k + \xi \right) \\ &= (n-1) \left(\frac{2\pi}{\lambda} d \cos \phi_k - \frac{2\pi}{\lambda} d \cos \phi_S \right), \end{aligned} \quad (3.7)$$

where $n = 1, 2, \dots, N_t$, and ϕ_k is the location of user k . As a result, the weight vector $\mathbf{w}_k[m]$ of Eq. (3.5) can be rewritten accordingly by substituting the values of $\psi_{n,k}$ in Eq. (3.7).

Random Beamforming

In the beamforming technique proposed in [6], the antenna phases $\psi_{n,k}[m]$ are random and independent of the location of the users. In other words, $\psi_{n,k}[m]$ is uniformly distributed in $[0, 2\pi]$, for $n = 1, 2, \dots, N_t$. We will label this technique *random beamforming* to stress upon the fact that the contribution of an antenna to the overall gain is independent of the contributions of all other antennas.

Beamforming Patterns

In the absence of fading, it is often useful to plot the overall channel gain versus the angle of departure ϕ , for a particular time slot m . In this case, $\mathbf{h}_k = \mathbf{1}_{N_t}$, and the normalized overall channel gain $\frac{1}{N_t}|\mathbf{g}_k|$ is thus given by $\frac{1}{N_t}|1 + e^{j\psi_{1,k}} + e^{j\psi_{2,k}} + \dots + e^{j\psi_{N_t-1,k}}|$. The polar plot of $\frac{1}{N_t}|\mathbf{g}_k|$ is often called the normalized beamforming pattern.

As shown in Fig. 3-3 and Fig. 3-4, the beamforming pattern of a ULA has two *main beams* of high gain, pointing in the direction of ϕ_S and $2\pi - \phi_S$. The smaller beams situated on either side of the main beams are called *side lobes*, and the directions in which the pattern's strength is zero are called *nulls*. Note that when we increase the number of antennas from $N_t = 2$ to $N_t = 4$, while keeping the separation d constant, more side lobes appear in the pattern and the main beam gets narrower.

In a nutshell, we can clearly see that in the absence of fading, changing the phase shift ξ at each time slot will produce a different beamforming pattern with directions receiving more power than others. However, we expect that on average, all directions will get the same power if the number of time slots is sufficiently large.

In the case of random beamforming, the beamforming pattern at a specific time slot looks totally random, even in the absence of fading. Indeed, as shown in Fig. 3-5, no direction is more privileged than the other, and the gain at each direction depends solely on the random phases generated at each antenna.

3.3 Dumb antennas and Multiuser Diversity

In this section, we show that multiuser diversity can be achieved by using dumb antennas and an appropriate scheduler. We consider both Rayleigh and Rician fast fading channels, and show that the use of dumb antennas leads to an improvement in performance only in

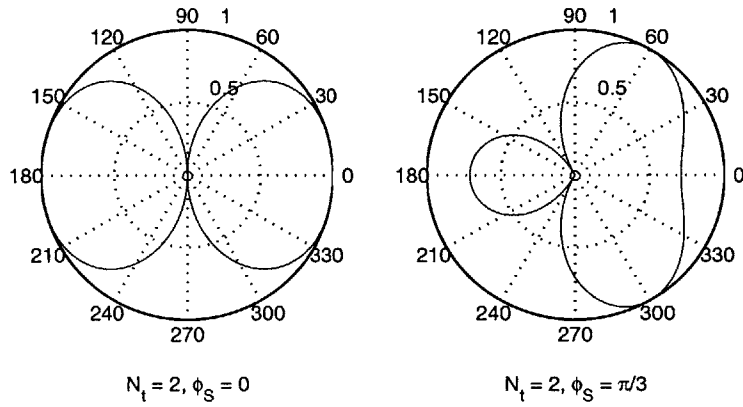


Figure 3-3: ULA normalized beamforming pattern for $N_t = 2$ transmit antennas with $d = \lambda/2$

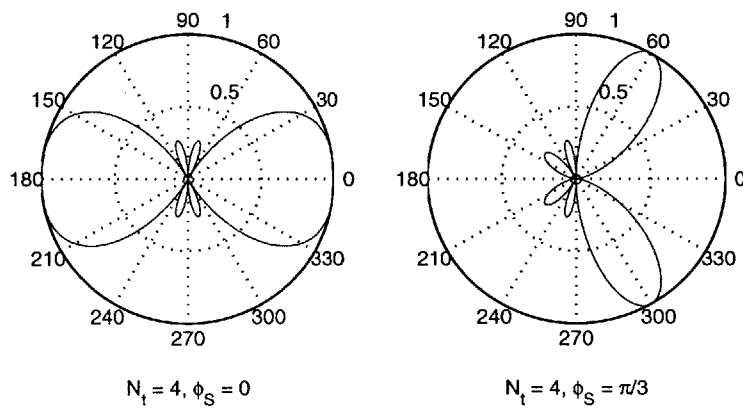


Figure 3-4: ULA normalized beamforming pattern for $N_t = 4$ transmit antennas with $d = \lambda/2$. Note that by increasing the number of antennas from 2 to 4, the main beam gets narrower, and side lobes begin to appear

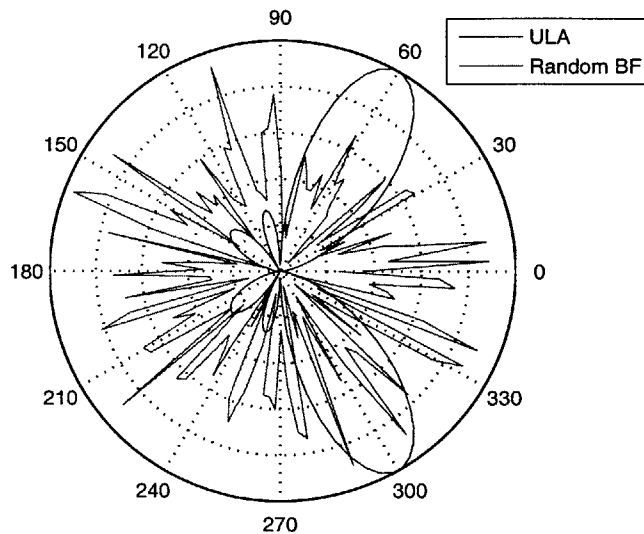


Figure 3-5: ULA and random beamforming normalized beamforming patterns for $N_t = 4$ transmit antennas with $d = \lambda/2$

the latter case.

3.3.1 Multiuser Diversity

Generally speaking, *diversity* is a technique for improving the reliability of communication between a sender and a receiver, by utilizing two or more signal paths that fade independently. Diversity plays a central role in combatting fading, and many diversity classes exist, such as time diversity (multiple versions of the same signal are transmitted over different time slots), frequency diversity (the signal is transmitted over different frequency channels) and space diversity (the signal is transmitted over different paths).

Multiuser diversity is another diversity class that operates at the system level rather than the user level, and that exploits fading instead of combatting it [6]. The goal is to maximize the overall throughput of the system by communicating to the user that can best exploit the channel resources [6] at a given time instance.

Choosing which user to transmit to at a particular time is handled by the *scheduler*, and a tradeoff between throughput and fairness is inevitable. For instance, the scheduler could assign time slots to each user in equal portions and in order, handling all users without

priority; in this case it is called a “round-robin” scheduler. This is a fair scheduler, but does not necessarily exploit the channel resources efficiently. Another type of scheduler would transmit to the user that currently has the best channel among all users. Even when the users have the same fading statistics, two users could have different average signal-to-noise ratios, due perhaps to different distances from the base station [5], or because of very disparate channel gains. Consequently, this scheduler lacks fairness since some users might never be scheduled.

Multuser diversity can be achieved by using the proportional fair scheduler (PFS) proposed in [6]. This algorithm transmits to the user that has the best channel with respect to its *own* average. As we have previously mentioned, the base station need not know the location of the users nor their individual channel coefficients.

Each user k feeds back only the throughput that its channel can support, or equivalently, the overall received SNR of its own channel, given by

$$\text{SNR}_k[m] = \frac{|\mathbf{h}_k^\dagger \mathbf{w}_k[m]|^2}{N_0}, \quad (3.8)$$

and the base station schedules transmission to the user \hat{k} with the highest SNR with respect to its own average $\overline{\text{SNR}}$, i.e.

$$\hat{k} = \arg \max_k \left\{ \frac{\text{SNR}_k[m]}{\overline{\text{SNR}}_k} \right\} \quad k = 1, 2, \dots, K. \quad (3.9)$$

3.3.2 Assumptions

In the sequel, we suppose that the following assumptions hold:

- There are $N_t = 2$ transmit antennas at the base station, aligned on the horizontal axis, and separated by a distance $d = \lambda/2$.
- There are K users in the system, and all of them are situated at the *same* distance R from the base station; we assume that $R \gg d$ so that the far field assumptions apply.
- Independent, fast fading: the users’ channels fade rapidly and independently.

3.3.3 Rayleigh Fading

We start by considering the independent Rayleigh fading model, whereby the individual channel coefficients are i.i.d. and $h_{n,k}[m] \sim \mathcal{CN}(0, \sigma^2)$. This means that the overall channel coefficients $\mathbf{h}_k[m]^\dagger \mathbf{w}_k[m]$, $k = 1, 2, \dots, K$, are independent across all users, and follow a Gaussian distribution regardless of the choice of $\mathbf{w}_k[m]$ [5].

This says that the distribution of the channel gain does not change if we increase the number of antennas, or whether we use ULA or random beamforming.

Distribution of the overall channel gain

In Fig. 3-6 we plot the kernel density function of the overall channel gain of one user in the system. In the case of ULA beamforming, we are plotting the density of the following quantity:

$$|h_{1,k}w_{k,1} + h_{2,k}w_{k,2}| = |h_{1,k}\sqrt{\alpha_1} + h_{2,k}\sqrt{\alpha_2}\exp[j(\pi \cos \phi_k + \xi)]|, \quad (3.10)$$

where α_1 and $\alpha_2 = 1 - \alpha_1$ vary between 0 and 1, and ξ varies uniformly between 0 and 2π , whereas in the random beamforming case, we are plotting the density of

$$|h_{1,k}w_{k,1} + h_{2,k}w_{k,2}| = |h_{1,k}\sqrt{\alpha_1}\exp(j\psi_1) + h_{2,k}\sqrt{\alpha_2}\exp(j\psi_2)|, \quad (3.11)$$

where ψ_1 and ψ_2 vary uniformly and independently between 0 and 2π .

As we expected, there is no essential difference between the two cases, and the distribution of the overall channel gain is identical to the case where there is only one transmit antenna. Consequently, using dumb antennas in a fast Rayleigh-faded system does not lead to any improvement over the single antenna case.

Average Received Power

In Fig. 3-7 we plot the mean received power, $\mathbb{E}[|\mathbf{h}_k[m]^\dagger \mathbf{w}_k[m]|^2]$, versus the angle of departure ϕ , for both ULA and random beamforming. We can see that there is no privileged location, and that on average, all user positions will receive roughly the same power, regardless of whether we use ULA or random beamforming. Also note that the grand mean over all powers is equal to 1, which was achieved by choosing $\alpha_1 + \alpha_2 = 1$.

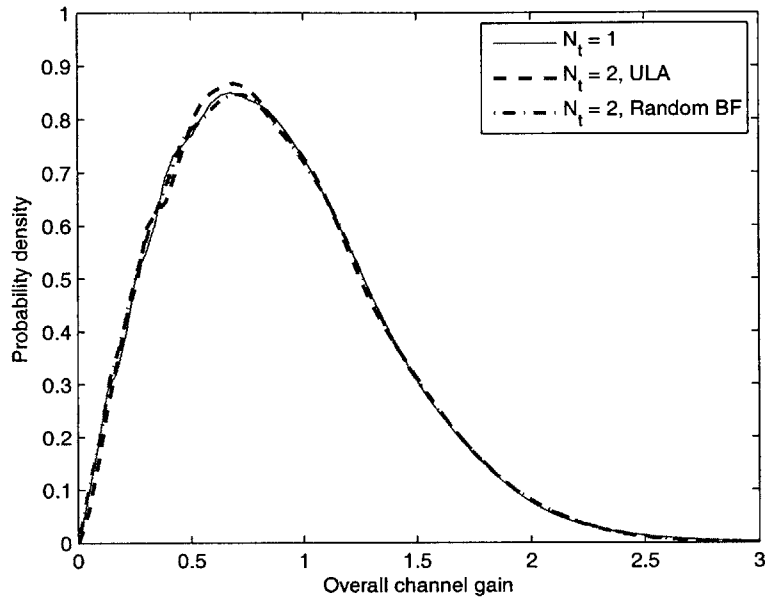


Figure 3-6: Rayleigh fading – Comparison of the distributions of the overall channel gains for one user. There is no essential difference between ULA and random beamforming, or between using 2 antennas versus 1 antenna

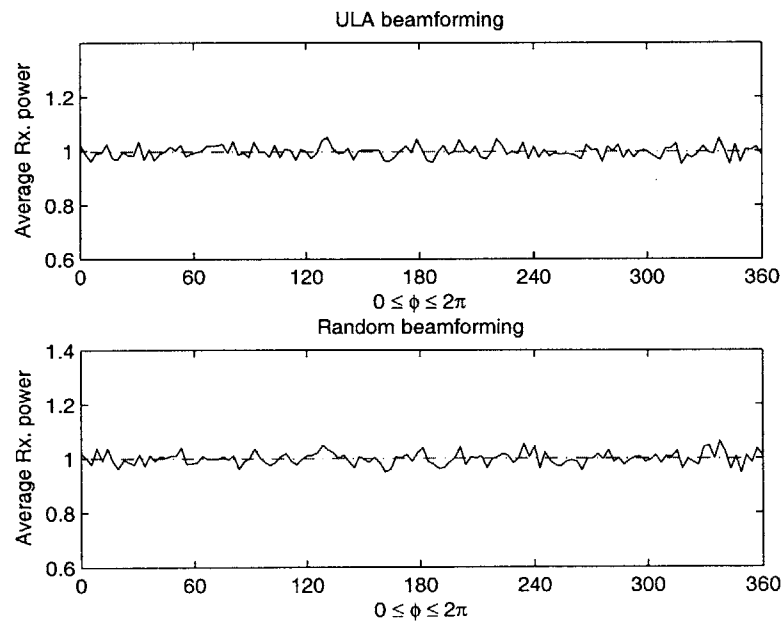


Figure 3-7: Rayleigh fading – Comparison of the mean received power versus ϕ , between ULA and random beamforming

Overall Channel Gain and Scheduling

In this paragraph, we consider a system with $K = 5$ users and investigate the performance of the proportional fair scheduler (PFS). In Fig. 3-8 we plot the overall channel gain of user 1 versus time, over a total duration of 120 time slots. The small squares correspond to the values of the gain at the times when the user is scheduled by the PFS, i.e. when the user has the best gain compared to its own average. As we can see, this specific user has been scheduled 25 times during that interval, or equivalently 20.8% of the time, which is approximately equal to $1/5$. Similar plots further substantiate the fairness of the PFS by showing that each of the remaining users will be scheduled roughly 20% of the time.

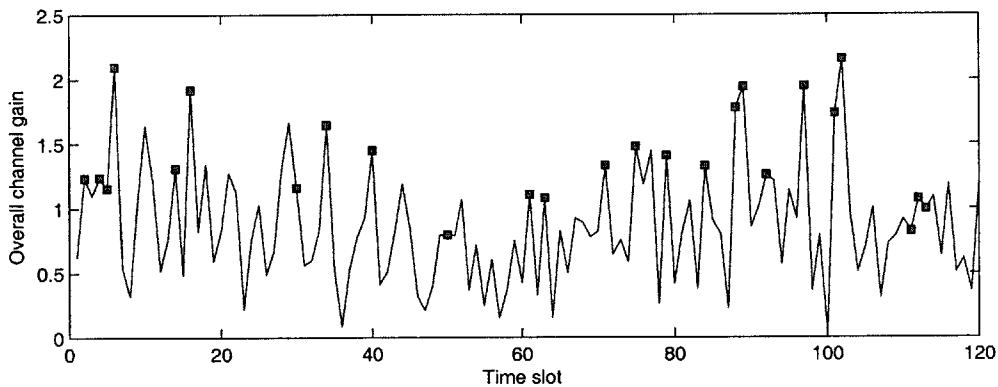


Figure 3-8: Rayleigh fading – Overall channel gain of user 1 versus time, for $K = 5$. The small squares correspond to the times when the user is being scheduled for transmission

3.3.4 Rician Fading

The Rayleigh model is extensively used in the literature to model wireless fading channels. Nevertheless, this model is often not sufficient to describe many channels found in the real world, and other models are used instead. One such model is the Rician fading, and is appropriate when there is a strong dominant (LOS) component between the transmitting antenna and the user, coupled with a scattered Rayleigh component.

The ratio of the energy in the dominant path to the energy in the diffused paths is denoted by κ and is often called the K -factor. For a fixed κ , the channel strength between antenna n and user k , at time m , can be written as [5]

$$h_{n,k}[m] = \sqrt{\frac{\kappa}{\kappa+1}}\sigma e^{j\varphi_{n,k}} + \sqrt{\frac{1}{\kappa+1}}\mathcal{CN}(0, \sigma^2) \quad (3.12)$$

The first term corresponds to the dominant path arriving with a uniform phase $\varphi_{n,k}$ and amplitude $\sqrt{\frac{\kappa}{\kappa+1}}\sigma$, whereas the second term refers to the usual Rayleigh component having Gaussian real and imaginary components with variance $\sigma^2/2$ each. In what follows, we assume that the dominant component of the fading is fixed between antenna n and user k , so that the Gaussian part is the only varying component. Note that for $\kappa = 0$ we can recover the Rayleigh fading, and for $\kappa \rightarrow \infty$, the fading is purely deterministic.

Distribution of the Overall Channel Gain

We saw in the Rayleigh fading case that the use of dumb antennas does not provide any gain in performance. However, significant gains can be achieved in a Rician environment, especially when the K-factor is large [5]. Indeed, the random variation in the phases $\psi_{n,k}$ and attenuations α_n helps create fluctuations in the LOS component, and the stronger this component is (larger κ), the larger the fluctuations become.

This intuition is corroborated in Fig. 3-9 and 3-10. In these figures, we plot the kernel density function of the overall channel gain of one user for $\kappa = 10$ and $\kappa = 100$, respectively. The following conclusions can be drawn:

- Contrary to the Rayleigh fading case, dumb antennas can increase the dynamic range of fluctuations in the presence of Rician fading.
- Since we are using only two transmit antennas, there is no essential difference in performance between ULA and random beamforming.
- When we increase the K-factor from 10 to 100, larger gains, relative to the single antenna case, can be achieved.

Average Received Power

In Fig. 3-11 we plot the mean received power versus ϕ . As in the Rayleigh fading case, we see that on average, all locations will receive the same power, regardless of whether we use ULA or random beamforming.

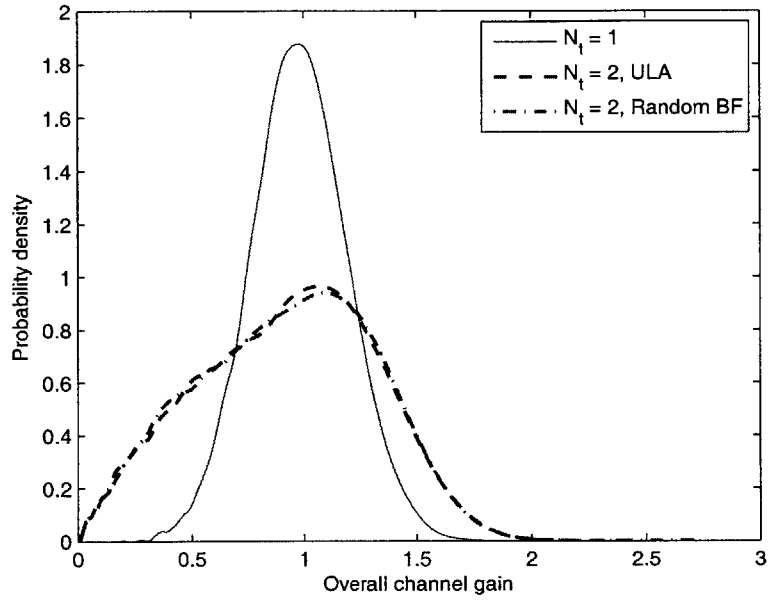


Figure 3-9: Rician fading – Comparison of the distributions of the overall channel gains for one user, for $\kappa = 10$

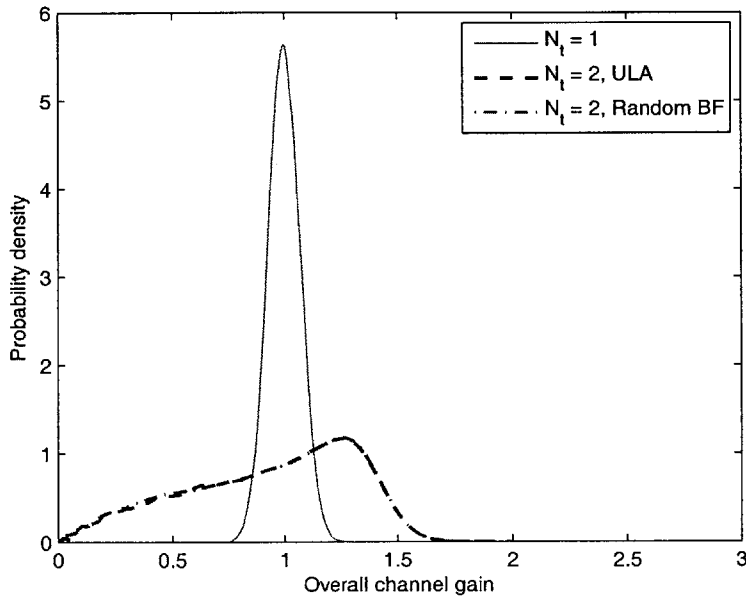


Figure 3-10: Rician fading – Comparison of the distributions of the overall channel gains for one user, for $\kappa = 100$

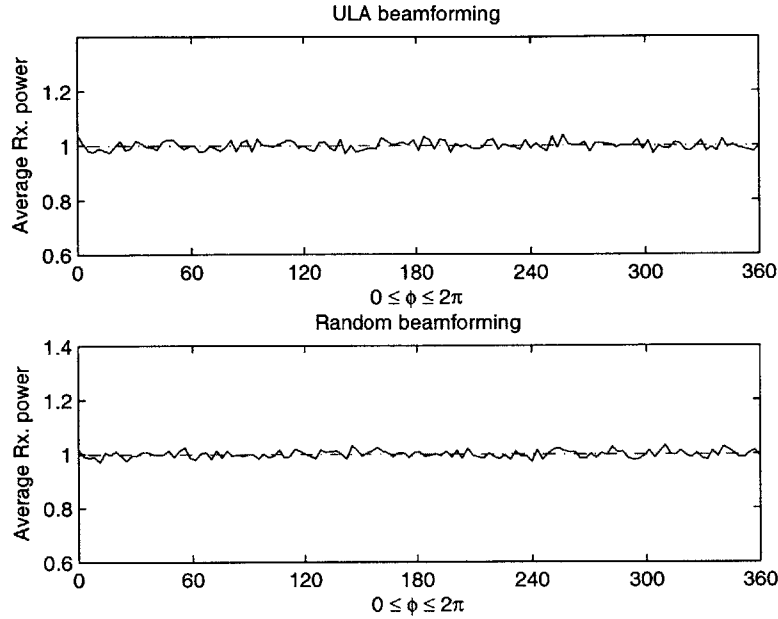


Figure 3-11: Rician fading – Comparison of the average received power versus ϕ , between ULA and random beamforming, for $\kappa = 10$

Overall Channel Gain and Scheduling

In this paragraph, we consider a system with $K = 5$ users and investigate the performance of the proportional fair scheduler (PFS). In Fig. 3-12 we plot the overall channel gain of user 1 versus time, over a total duration of 120 time slots. We can see that this user has been scheduled 21 times during that interval, or equivalently 17.5% of the time. The remaining users will also be scheduled roughly one fifth of the time, again proving the fairness of the PFS.

3.4 MATLAB Graphical Simulation

Fig. 3-13 through 3-15 show three screenshots of our MATLAB simulation of dumb antennas and beamforming in multiuser environments. The simulation efficiently amalgamates the concepts of beamforming, dumb antennas, multiuser fading channel and scheduling algorithms, in a simple and user-friendly interface.

We used a uniform linear array to perform the simulation. The interface includes five main sections:

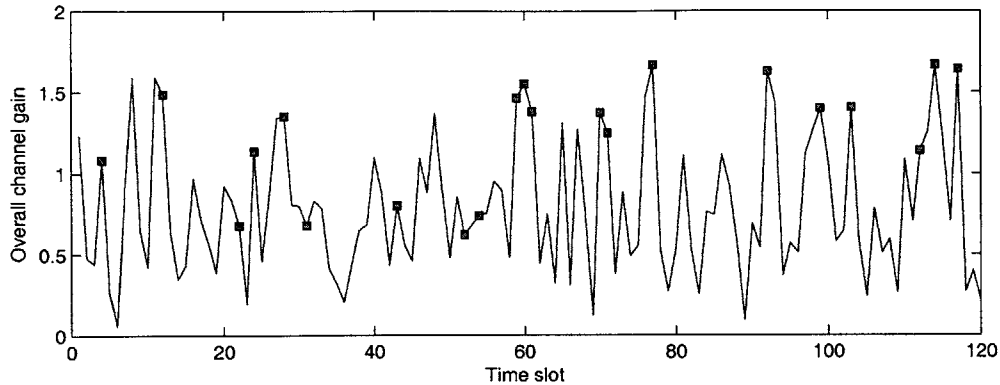


Figure 3-12: Rician fading – Overall channel gain of user 1 versus time, for $K = 5$ and $\kappa = 10$. The small squares correspond to the times when the user is being scheduled for transmission

- Simulation parameters:** this panel contains three important parameters that can be changed before running the simulation. These parameters are the number N_t of transmit antennas (2, 4 or 8), the number of users K (1, 5 or 10) and the fading distribution (Rayleigh or Rician). These variables can be saved by clicking on the Save Parameters button.
- Beamforming panel:** this panel contains a polar plot of the normalized beamforming pattern of the ULA antenna array. As the simulation is taking place, the plot updates the pattern at each time slot. Moreover, the users are represented by (fixed) small filled disks distributed randomly around the circle. At each time slot, the disk of the scheduled user will be colored in green, whereas all other users will be represented by the blue color.
- Control panel:** this panel contains three buttons that allow the user to start, pause or resume the simulation. The Start Animation button starts the simulation, whereas the Pause Animation and Resume Animation buttons pause it and resume it, respectively.
- Graph figure:** this graph plots the overall channel gain of user 1 versus time. The small squares indicate that the user has been selected for transmission by the proportional fair scheduler.
- Output panel:** after the simulation completes (we fixed the number of time slots to 120), the output panel displays the percentage of schedules for this user (this should

be around $1/K \times 100\%$), the average overall gain, and the average overall gain at the times where the user has been scheduled.

After the simulation ends (see Fig. 3-14), we can plot the distribution of the overall channel gain of the user (see Fig. 3-15). The Options → Reset menu item resets the initial parameters and allows us to run another simulation.

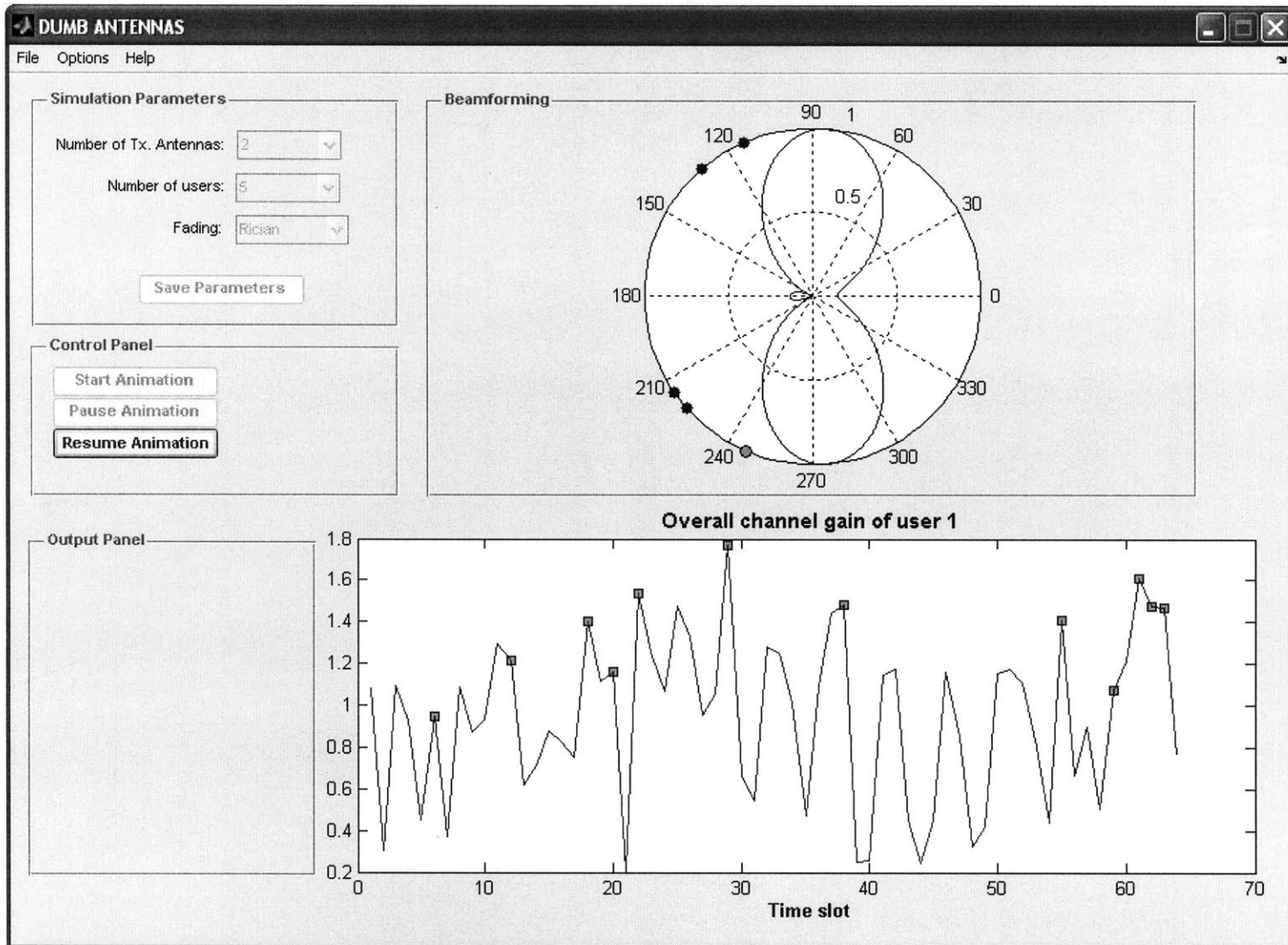


Figure 3-13: Dumb antennas – MATLAB graphical simulation. The beamforming and channel gain plots are updated dynamically as the simulation runs

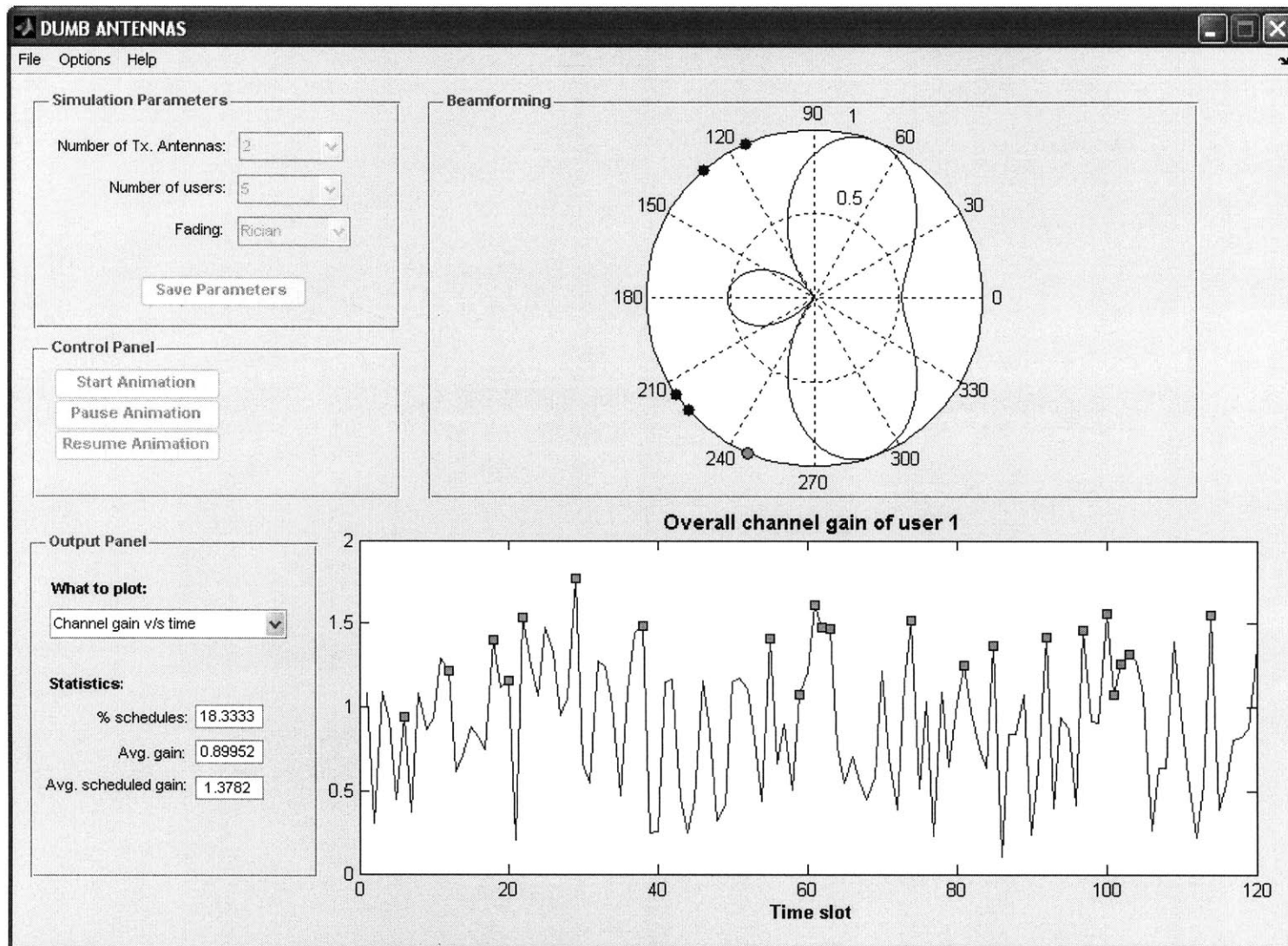


Figure 3-14: Dumb antennas – MATLAB graphical simulation. After the simulation completes, statistics about scheduling and the channel gain are displayed

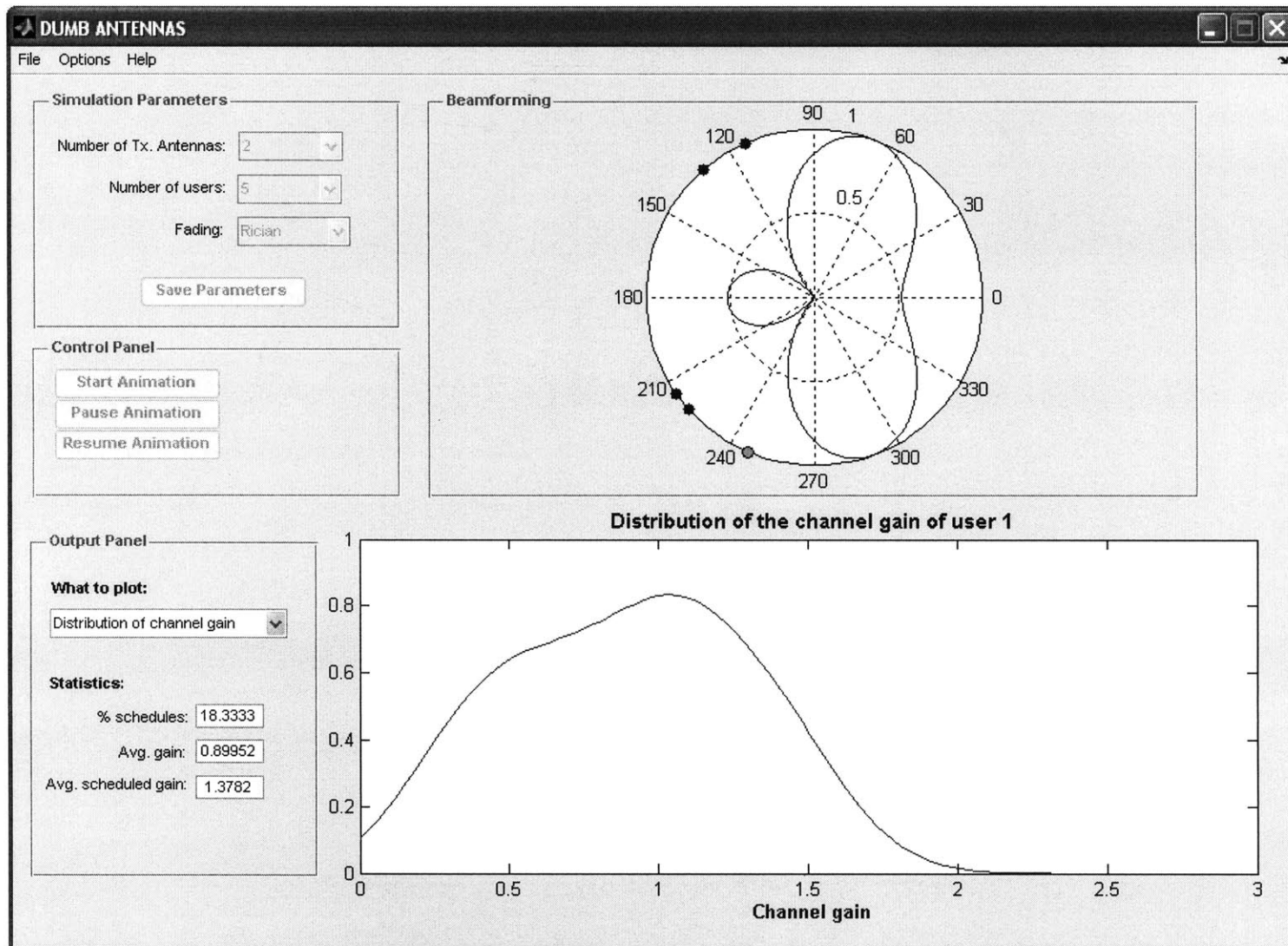


Figure 3-15: Dumb antennas – MATLAB graphical simulation. The distribution of the channel gain of user 1 can also be plotted after the simulation ends

Chapter 4

Underlying Principles of OFDM

In this chapter, we describe the underlying principles of orthogonal frequency division multiplexing (OFDM). In Sec. 4.1 we prove that sinusoids are the eigenfunctions of linear time-invariant systems. In Sec. 4.2 we give an overview of frequency-selective fading and describe the input-output relationship of this type of channel. In Sec. 4.3 we coalesce the development of the first two sections by explaining the motivation behind OFDM and proving, by simulation, the need for the cyclic prefix. Finally, in Sec. 4.4, we describe our MATLAB graphical simulation of OFDM.

4.1 Eigenfunctions of LTI Systems

We consider the linear time-invariant (LTI) system \mathcal{H} shown in Fig. 4-1. We denote by $h[m]$ the impulse response of the system, where m is the time index, and by $x[m]$ and $y[m]$ the input and output sequences, respectively.

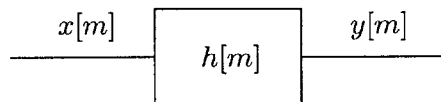


Figure 4-1: Discrete-time LTI system

It is well known that complex sinusoids are eigenfunctions of LTI systems. This means that the response to a sinusoid is another attenuated sinusoid of the same frequency. In other words, if the input is a sinusoid of frequency $f_0 = \frac{\omega_0}{2\pi}$, i.e. $x[m] = e^{j\omega_0 m}$, then $\mathcal{H}\{e^{j\omega_0 m}\} = \lambda \cdot e^{j\omega_0 m}$, where λ is an arbitrary constant. This can be proved straightforwardly

by noting that the discrete-time Fourier transform (DTFT) of $x[m]$ is equal to

$$X(\omega) = \sum_m x[m]e^{-j\omega m} = 2\pi\delta(\omega - \omega_0)$$

It follows that the DTFT of $y[m]$ is given by

$$\begin{aligned} Y(\omega) &= X(\omega)H(\omega) \\ &= 2\pi\delta(\omega - \omega_0) \cdot H(\omega) \\ &= 2\pi H(\omega_0) \cdot \delta(\omega - \omega_0) \\ &= \lambda \cdot \delta(\omega - \omega_0), \end{aligned}$$

where $\lambda = 2\pi H(\omega_0)$ is a constant. As a result, $y[m] = \text{DTFT}^{-1}\{\lambda \cdot \delta(\omega - \omega_0)\} = \lambda \cdot e^{j\omega_0 m}$, effectively proving that sinusoids are eigenfunctions of LTI systems.

4.2 Frequency-selective Fading

Consider a wireless channel of bandwidth \mathcal{W} , and denote its coherence bandwidth by \mathcal{W}_c . In the case where $\mathcal{W} > \mathcal{W}_c$, the channel is called frequency-selective, and the number of resolvable multipath components (channel taps) is $L \approx \mathcal{T}_d \mathcal{W}$, where \mathcal{T}_d is the delay spread of the channel.

The discrete-time representation of a frequency-selective channel can be described by a tapped-delay line model, as shown in Fig. 4-2. A unit time delay is denoted by D , and the noise $z[m]$ is assumed to be complex Gaussian. It follows that the system response at time m is given by

$$y[m] = \sum_{\ell=0}^{L-1} h_\ell[m]x[m - \ell] + z[m] \quad (4.1)$$

We further assume that the ℓ^{th} tap does not vary with time and thus the channel is linear time-invariant [5]. Therefore, Eq. (4.1) can be rewritten as

$$y[m] = \sum_{\ell=0}^{L-1} h_\ell x[m - \ell] + z[m] \quad (4.2)$$

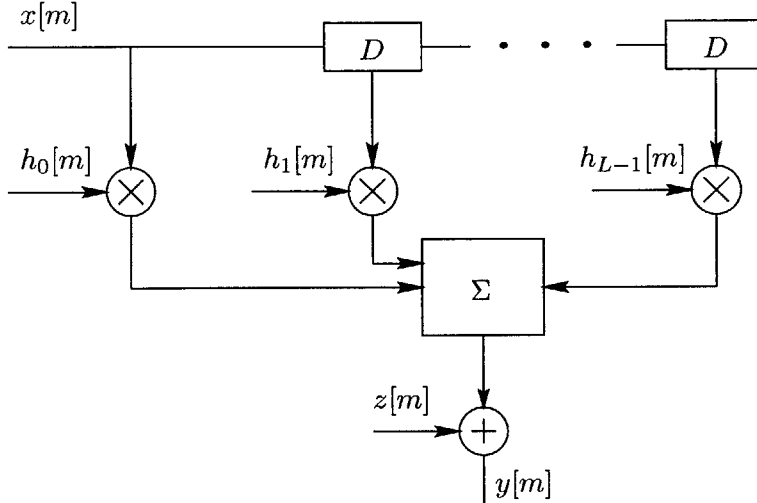


Figure 4-2: Tapped-delay line model. The output depends on attenuated and time-delayed copies of the input

4.3 Orthogonal Frequency Division Multiplexing (OFDM)

4.3.1 Motivation

Consider the frequency-selective, single-carrier channel of Eq. (4.2). In this scenario, the delay spread is typically of the order of the symbol period or larger, which means that the system experiences significant intersymbol interference (ISI). The effect of ISI can usually be mitigated by using complex equalization schemes.¹

However, if we break the channel into N subcarriers, where N is typically large, then each subchannel bandwidth $\mathcal{W}_N = \mathcal{W}/N$ would be small compared to \mathcal{W} [3]. If the subcarriers are orthogonal to each other, then the symbols on each subchannel could be demodulated without interference from other carriers. The system would thus behave as a collection of flat-fading subchannels, where both intersymbol and intercarrier interferences are negligible.

4.3.2 Orthogonal Subcarriers

As we showed in Sec. 4.1, if we transmit a sinusoid over an LTI system, the resulting response is another sinusoid of the same frequency. In OFDM, the subcarriers are sinusoids and possess this special property of being the eigenfunctions of the LTI channel. Furthermore,

¹Generally speaking, equalizers are filters that attempt to combat ISI by applying digital processing techniques on the received signal.

these sinusoids are chosen to be orthogonal to each other, thus practically eliminating intercarrier interference (ICI). Orthogonality between subchannels is ensured by carefully choosing the frequencies of the carriers and the pulse shaping filters.

4.3.3 Finite Duration Sinusoids

If we transmit a time-limited sinusoid over an LTI system, then the resulting output will no longer be a sinusoid. Fortunately, the channel impulse response can usually be treated as having a finite number of taps L , so orthogonality could be restored by ensuring that every subcarrier has an integer number of cycles over each OFDM symbol duration $T_N = TN$, where T is the single carrier symbol duration.

To see this more clearly, assume that the input to the channel is a finite-length sinusoid and that the channel coefficients are real Gaussian, $h_\ell \sim \mathcal{N}(\mu = 0, \sigma^2 = 1/2)$, $\ell = 0, 1, \dots, L - 1$. In Fig. 4-3, we plot the channel output versus time and compare it to the sinusoidal input, in the absence of noise, and for $L = 20$ taps. As we can see, $y[m]$ is distorted over the interval $1 \leq m \leq L$, which corresponds to the delay spread of the channel. Beginning at $m = L + 1$, the response starts to look as a sinusoid having the same frequency as the input.

4.3.4 Cyclic Prefix

A cyclic prefix is a special sequence that can be added to the beginning of the input sinusoid, and that consists its last L sample points. The function the cyclic prefix is two-fold:

- Restore the orthogonality between the subcarriers, by ensuring that each has an integer number of cycles over the interval $[0, T_N]$
- Remove any remaining ISI within each subcarrier by extending the length of the data sequence enough to cancel the effect of multipath spread.

In Fig. 4-4 we show that by adding a cyclic prefix at the beginning the sinusoid, we can disregard the first L symbols at the receiver, and only consider the remaining symbols of the output. Note that the output after time $m = 20$ is a sinusoid that has exactly 3 periods. A similar plot would show that if we remove the cyclic prefix at the receiver, all the subcarriers would effectively have an integer number of cycles over $[0, T_N]$, thus restoring orthogonality between them.

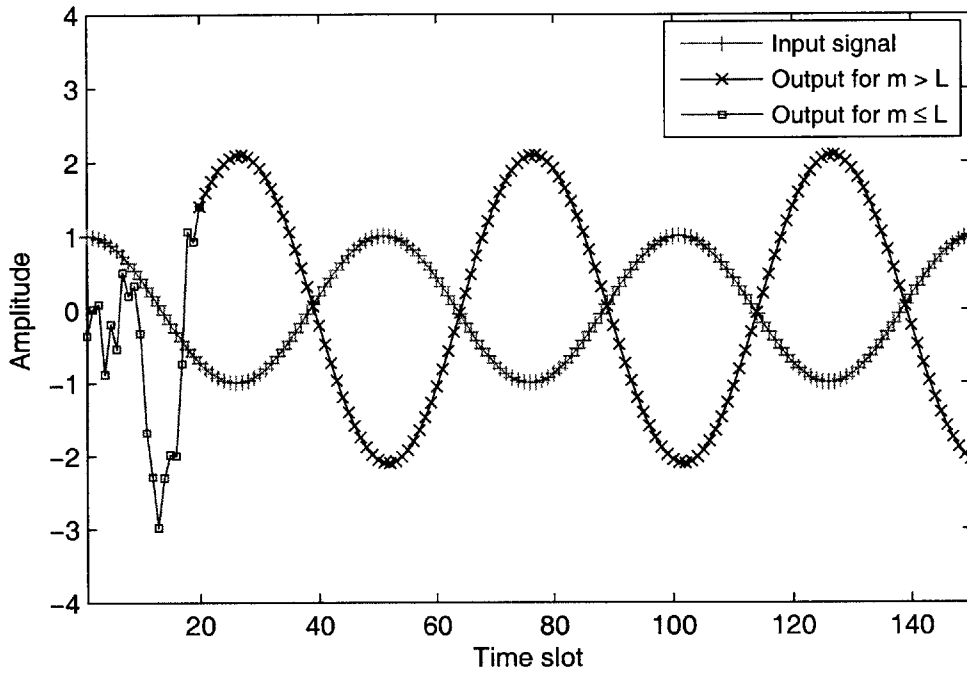


Figure 4-3: Input-output relationship in an LTI fading channel with $L = 20$ taps

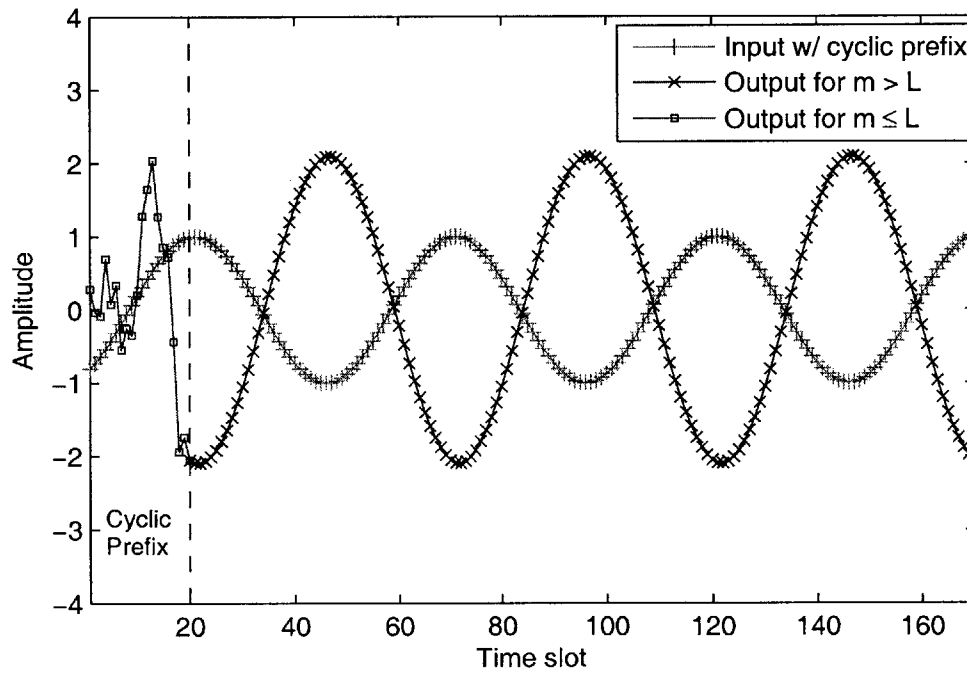


Figure 4-4: Input-output relationship after the addition of a cyclic prefix

4.4 MATLAB Graphical Simulation

The purpose of this simulation is to get a sense of why a time-limited input sinusoid is no longer an eigenfunction of an LTI channel. We are evaluating this observation in the context of OFDM, for our channel input is actually a sinusoidal subcarrier of an OFDM system. OFDM restores the eigenfunction property by adding a cyclic prefix to the subcarrier, which both eliminates ISI and ensures that all subchannels are orthogonal to each other. We tried to abstract this intuitive idea of multicarrier systems, for the actual digital implementation of OFDM is quite complicated, and involves dealing with Fourier transforms at both the sender and receiver.

In this simulation, we are considering only one sinusoidal subcarrier and observing the effects of multipath fading on the subchannel's output. The total duration of the simulation is 150 time slots, and the input has 3 cycles in this time interval. The channel taps are independently distributed real Gaussian variables, each with mean 0 and variance 1/2, and the number of taps is chosen to be $L = 20$. Note that the number of taps is usually much smaller than 20, but we purposely used a large number in order to better assess the effect of multipath fading, and to better highlight the ability of the cyclic prefix to combat it.

Fig. 4-5 and 4-6 show two screenshots of our MATLAB simulation of OFDM. The interface includes two main parts:

- **Control panel:** this panel contains three buttons. The Start button uses the saved parameters² to start the simulation. The button Add Cyclic Prefix – which can only be pressed after the simulation ends – adds a cyclic prefix to the input sinusoid and redraws both the input and output. The button Remove Cyclic Prefix restores the original configuration that has no prefix.
- **Graph figures:** the top figures plot a sinusoidal subcarrier input and the corresponding output versus time, respectively. These are plotted dynamically as the time index increases from 1 to 150. The bottom figure shows the channel taps magnitude versus time.

²These parameters are not shown on the interface, but include the input frequency, the number of taps L , the number of time slots, and the channel distribution, among others

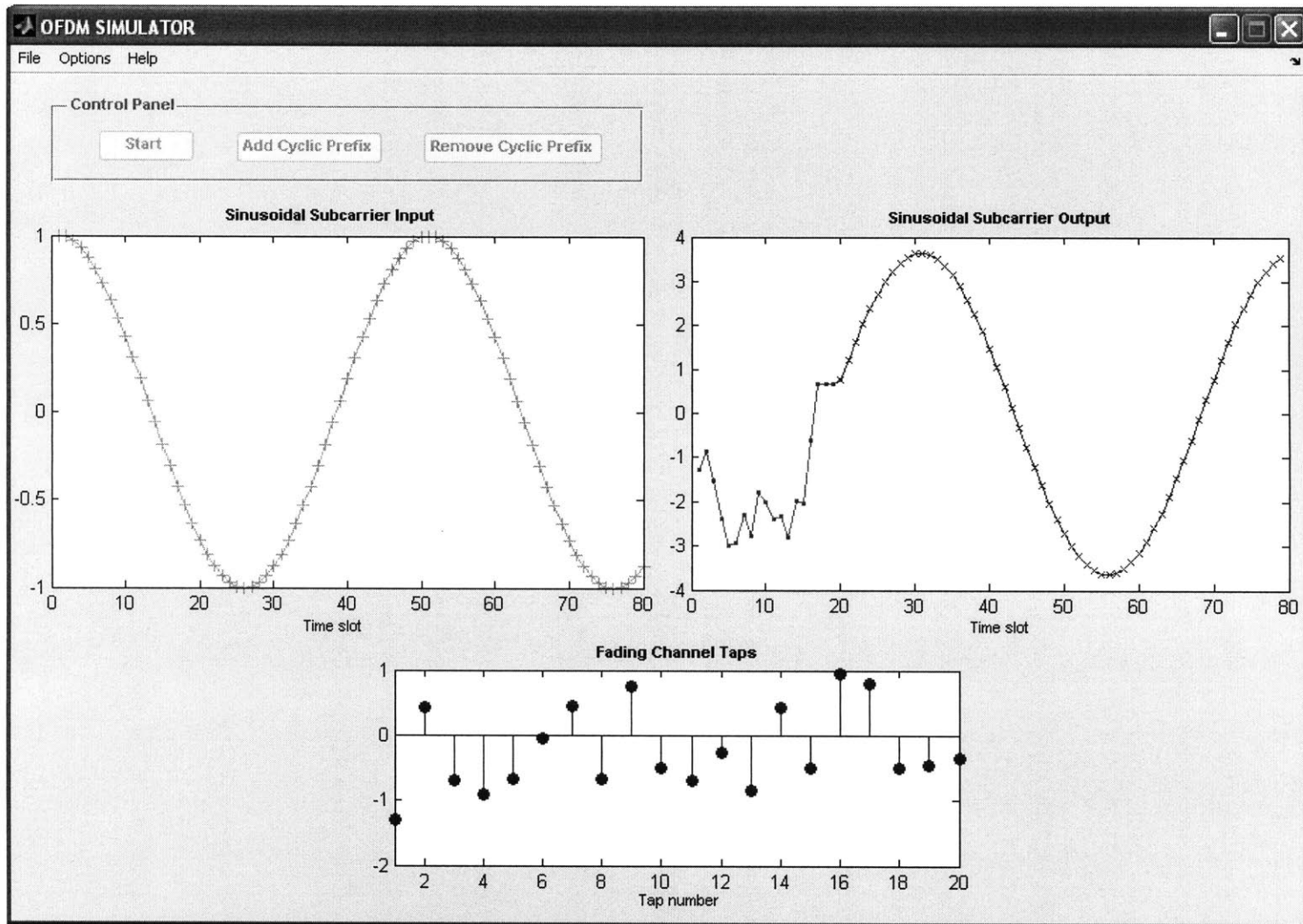


Figure 4-5: OFDM – MATLAB graphical simulation. The top figures dynamically plot the input and output sample points of one subcarrier

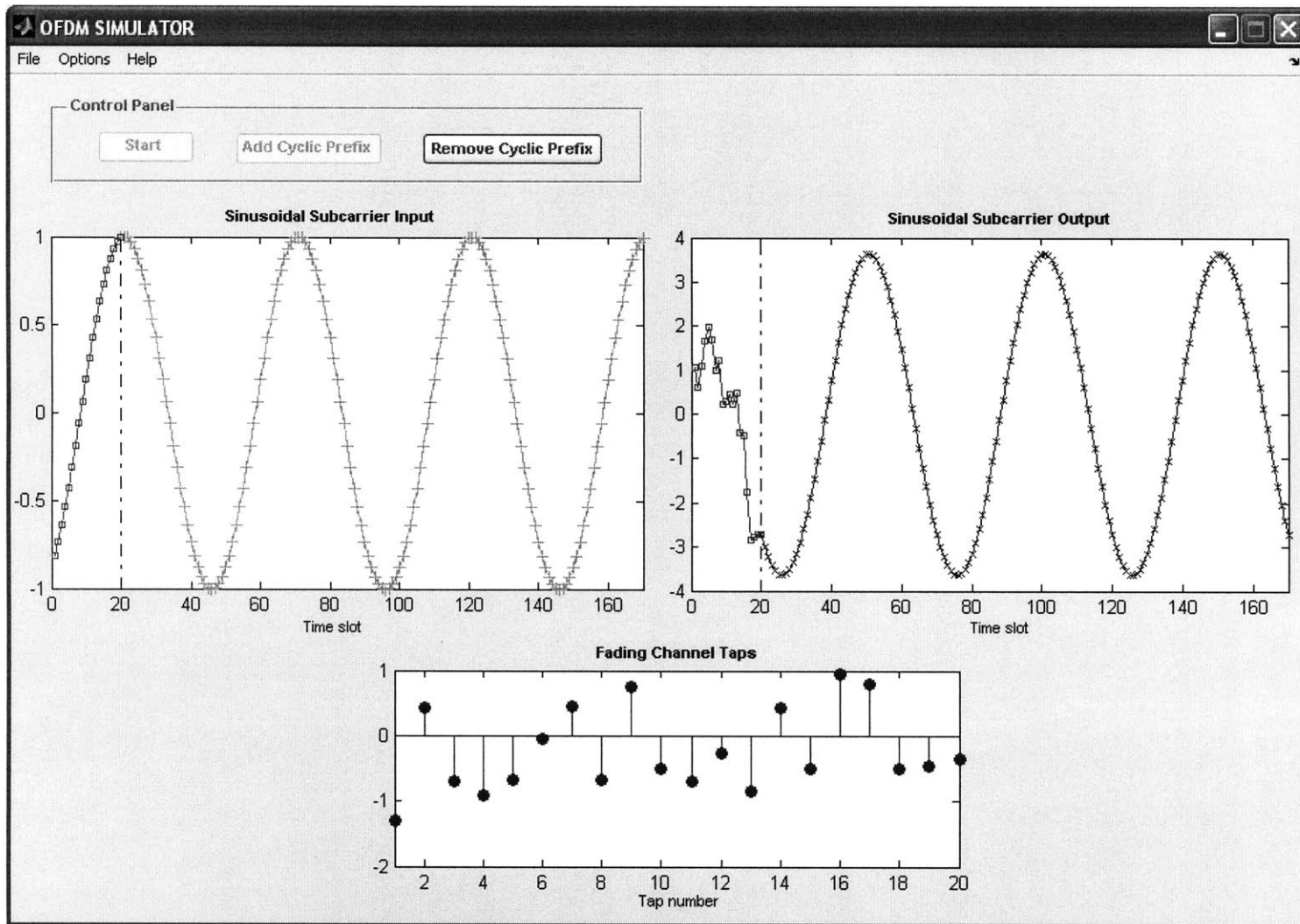


Figure 4-6: OFDM – MATLAB graphical simulation. After the simulation ends, the Add Cyclic Prefix button updates the input and output figures accordingly

Chapter 5

Conclusion

5.1 Summary

This thesis presented a set of simulations for models and algorithms in wireless communications. The simulations involved topics of central importance in wireless systems and presented them in user-friendly, graphical MATLAB interfaces. The topics included wireless channel modeling and statistical analysis, antenna beamforming in multiuser fading environments and orthogonal frequency division multiplexing.

These simulations target two types of audiences in particular: students and wireless industry professionals. Typically, they may be demonstrated in undergraduate or graduate classrooms as a visual complement to lecture notes, or used individually by students and engineers in order to better understand key aspects of wireless channels and technologies.

The motivation of this thesis emanates from the fact that understanding wireless communications can often be hindered by complicated mathematical details. This manuscript abstracted the physical aspects and underlying principles of wireless systems, in an attempt to make their comprehension easier and more intuitive.

Although our MATLAB code dealt with complex derivations and algorithms, the resulting simulations were simple and easy to use. The educational value of the thesis lies in the fact that it allows students and engineers to visualize wireless phenomena and quantities without having to deal with tedious derivations.

5.2 Future Work

It was difficult to implement all important concepts in wireless communication, for this area is immense and rapidly evolving. In the near future, we intend to simulate the underlying concepts of spread-spectrum modulation, which is the cornerstone of many state-of-the-art wireless systems such as CDMA and UMTS. Demonstrating the fundamentals of cellular systems is an idea that we would like to implement as well. Our ultimate objective is to have a complete set of simulations that serve as an effective visual material for introductory classes, and as a simple yet important complement for students in more advanced courses.

Bibliography

- [1] David K. Cheng. *Fundamentals of Engineering Electromagnetics*. Addison-Wesley, 1993.
- [2] Robert G. Gallager. Principles of digital communication. MIT 6.450 course notes, November 2005.
- [3] Andrea Goldsmith. *Wireless Communications*. Cambridge University Press, 2005.
- [4] Andreas F. Molisch. *Wireless Communications*. Wiley-IEEE Press, 2005.
- [5] David Tse and Pramod Viswanath. *Fundamentals of Wireless Communication*. Cambridge University Press, 2005.
- [6] Pramod Viswanath, David N. C. Tse, and Rajiv Laroia. Opportunistic beamforming using dumb antennas. *IEEE Transactions on Information Theory*, 48(6), June 2002.